REPORT 1107

AN EMPIRICALLY DERIVED BASIS FOR CALCULATING THE AREA, RATE, AND DISTRIBUTION OF WATER-DROP IMPINGEMENT ON AIRFOILS [1]

By Norman R. Bergrun

SUMMARY

An empirically derived basis for predicting the area, rate, and distribution of water-drop impingement on airfoils of arbitrary section is presented. The concepts involved represent an initial step toward the development of a calculation technique which is generally applicable in the design of thermal ice-prevention equipment for airplane wing and tail surfaces. It is shown that sufficiently accurate esitmates, for the purpose of heated-wing design, can be obtained by a few numerical computations once the velocity distribution over the airfoil has been determined.

The calculation technique presented is based on results of extensive water-drop trajectory computations for five airfoil cases which consisted of 15-percent-thick airfoils encompassing a moderate lift-coefficient range. The differential equations pertaining to the paths of the drops were solved by a differential analyzer.

INTRODUCTION

The design of thermal ice-prevention equipment for airplane wing and tail surfaces has progressed to the point where the amount and distribution of heat flow can be calculated for specified flight and icing conditions (reference 1). This design procedure requires information as to the area, rate, and distribution of water-drop impingement on the leading edge of the airfoil section being analyzed. In the past, area and rate of water-drop impingement have been estimated by using a method involving the substitution of a circular cylinder for the airfoil leading edge, as suggested in references 1 and 2. This substitution method is adequate for design purposes for some combinations of cylinder diameter and drop size, but it can produce sizable errors for other combinations (references 1, 3, and 4).

A second means of estimating the area and rate of water-drop impingement on airfoils is provided by reference 3. This method is more accurate than the cylinder substitution method, but the calculation procedure is somewhat laborious and, as a result, its use is not too practicable in a complete design study where a large number of water-drop trajectories are usually required.

To establish a procedure which would eliminate the laborious computations of water-drop trajectories in the design of wing thermal ice-prevention equipment, it became apparent that a large number of water-drop trajectories would be required for study. Experience with calculating trajectories by the method of reference 3 had shown that the pattern of water-drop impingement for drop sizes usually encountered in flight can be related most directly to velocity distribution over the surface of the airfoil. Airfoil shape itself appeared to have an effect on the pattern of impingement, but to a lesser degree than velocity distribution. Five airfoil cases were chosen as being the minimum which could be expected to provide sufficient data to include the effects of these two factors. Water-drop trajectories were computed for these five cases.

This report presents some of the results of the water-drop-trajectory computations described in detail in reference 5 (NACA TN 2476, 1951). In addition, the method derived empirically in reference 5 for rapidly estimating area, rate, and distribution of water-drop impingement is discussed. The limitations of this method and the technique employed in its use are also presented herein.

SYMBOLS

The following nomenclature is used throughout this report:

a	airfoil mean-line designation, fraction of chord from leading edge over which design load is uniform
a_d	instantaneous drop-acceleration ratio, dimensionless
A_o	area normal to flow direction outlined by several trajectories at free-stream conditions, square feet
A_s	area of impingement outlined on an airfoil surface by trajectories starting at free-stream conditions from an initial area of A_o, square feet
c	chord length of airfoil, feet
C	concentration factor $\left(\frac{dA_o}{dA_s}\right)$, dimensionless
C_d	drag coefficient of drop, dimensionless
c_l	section lift coefficient, dimensionless
E	collection efficiency of airfoil based on airfoil maximum thickness, percent
G	rate of change of velocity along the stagnation streamline at the stagnation point $\left[\frac{d(U_a/V)}{dS}\Big\|_{\psi=0}\right]$, dimensionless
h	frontal height of airfoil, fraction of chord
k	slope of airfoil contour at a particular chordwise position, dimensionless
L	length of span, feet
m	liquid-water content of icing cloud, pounds of water per cubic foot of air

[1] Summarizes material presented in NACA TN 2476 entitled "An Empirical Method Permitting Rapid Determination of the Area, Rate, and Distribution of Water-Drop Impingement on an Airfoil of Arbitrary Section at Subsonic Speeds," by Norman R. Bergrun, 1951.

M_a weight rate of water-drop impingement per unit of surface area, pounds per hour, square foot

M_s weight rate of impingement of water drops on a body, per unit span, pounds per hour, foot

P ratio of the vector difference between the local air and drop velocities to free-stream velocity $\left(\frac{\overline{U}_a-\overline{U}_d}{V}\right)$, dimensionless

r radius of drop, feet

R Reynolds number for drop at relative velocity PV $\left(\frac{2PVr}{\nu}\right)$

R_V Reynolds number for drop at free-stream velocity V $\left(\frac{2Vr}{\nu}\right)$

s distance along airfoil surface from leading edge, positive on upper surface and negative on lower surface, feet

S distance along water-drop trajectory, fraction of chord

t time, seconds

t_e equivalent ellipse thickness ratio for a low-drag airfoil $\left(\frac{2\rho}{t_{max}}\right)$, fraction of chord

t_{max} maximum thickness of airfoil, fraction of chord

u component of local velocity parallel to chord line, feet per second

U local velocity of air or drop, feet per second

v component of local velocity perpendicular to chord line, feet per second

V free-stream air velocity, feet per second

x,y rectangular coordinates for a system of axes having the origin at the airfoil leading edge and the x axis, positive toward the trailing edge, lying along the airfoil chord, fraction or percent of chord.

x', y' retangular coordinates for a system of axes having the origin at the airfoil leading edge and the x' axis, positive in the free-stream direction, lying parallel to free-stream direction, fraction or percent of chord

Δy total airfoil-ordinate intercept established by two impinging trajectories starting from infinity at a distance Δy_o apart, fraction of chord

Δy_o distance between two trajectories at infinity, fraction of chord

$\Delta y_o'$ distance between two trajectories at infinity measured in x',y' coordinates, fraction of chord

Δy_{o_t} distance between two trajectories which start at infinity and impinge tangentially on the airfoil, fraction of chord

α angle of attack, degrees

γ specific weight, pounds per cubic foot

θ angular displacement between local velocity and x axis, degrees

ν kinematic viscosity of air, square feet per second

ρ airfoil leading-edge radius, fraction of airfoil chord

τ time scale $\left(\frac{tV}{c}\right)$, dimensionless

ψ scale modulus $\left(9\frac{\gamma_a}{\gamma_d}\frac{c}{r}\right)$, dimensionless

Ψ stream function, dimensionless

SUBSCRIPTS

a air

av average

cr critical

d drop

e effective

l lower surface

max maximum

o initial condition

s condition at airfoil surface

t tangential

u upper surface.

DERIVATION OF THE METHOD

The method derived in NACA TN 2476 for calculating area, rate, and distribution of drop impingement assumes that airfoil velocity distribution is the primary factor influencing the paths of water drops which approach an airfoil. This assumption is an outgrowth of experience in calculating water-drop trajectories by the method of reference 3, and it permits the study of water-drop trajectory characteristics according to the factors which influence airfoil pressure distribution.

DESCRIPTION OF PROCEDURE USED TO OBTAIN WATER-DROP TRAJECTORIES

Five airfoil cases were selected as being the minimum number which reasonably could be expected to provide sufficient data for showing the effects on water-drop trajectories of altering airfoil velocity distribution. These cases are listed in table A.

TABLE A.—AIRFOIL CASES CONSIDERED IN WATER-DROP-TRAJECTORY STUDY OF NACA TN 2476

Case	Airfoil	Angle of attack, α (deg)	c_l	Leading-edge radius, ρ (percent chord)
1	15-percent-thick symmetrical Joukowski	0	0	2.07
2	do	2	.22	2.07
3	do	4	.44	2.67
4	15-percent-thick cambered Joukowski	0	.44	2.67
5	NACA 65_A-015 (symmetrical)	4	.44	1.505

Table A shows the systematic changes in the variables which affect velocity distribution. Cases 1, 2, and 3 were intended to reveal the effects of altering airfoil velocity distribution by changing angle of attack; case 4, compared to cases 1 and 3, the effects of altering velocity distribution by the addition of a basic load distribution obtained by cambering the mean line; and cases 3 and 5, the effects of changing general airfoil shape for a given angle of attack and lift coefficinet. The upper- and lower-surface velocity distributions over the forward region of each of the five airfoils are shown in figure 1. Velocity distributions for several Joukowski airfoils are used because the required velocity components in the field of flow are more readily calculated than for other airfoils. It is noted in figure 1 that the variables selected did not result in a

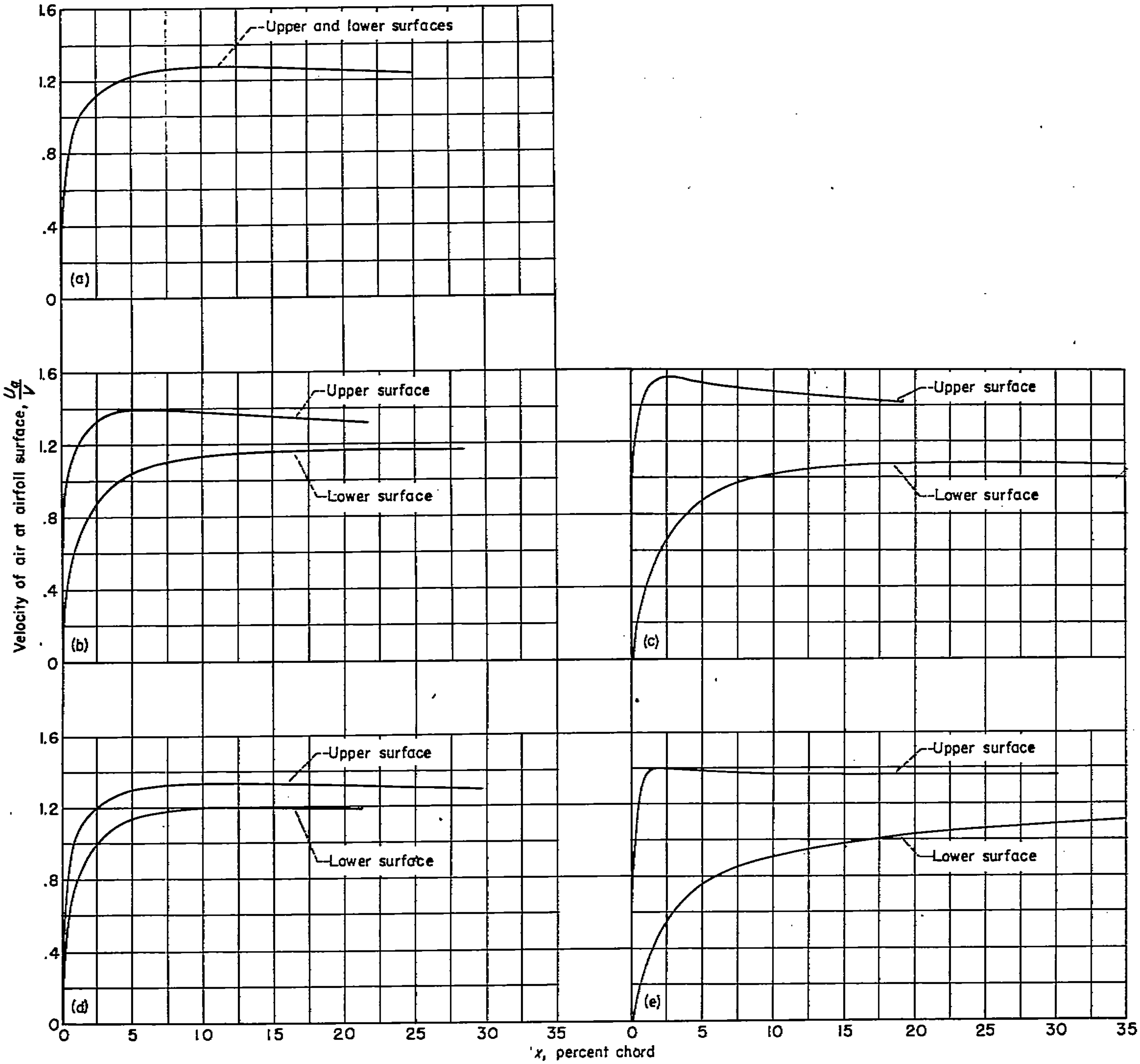

(a) Symmetrical 15-percent-thick Joukowski airfoil; $c_l=0$; $\alpha=0°$.
(b) Symmetrical 15-percent-thick Joukowski airfoil; $c_l=0.22$; $\alpha=2°$.
(c) Symmetrical 15-percent-thick Joukowski airfoil; $c_l=0.44$; $\alpha=4°$.
(d) Cambered 15-percent-thick Joukowski airfoil; $c_l=0.44$; $\alpha=0°$; $a=1.0$ mean line.
(e) NACA 65_1-015 airfoil; $c_l=0.44$; $\alpha=4°$.

FIGURE 1.—Airfoil velocity distributions for the five airfoil cases comprising the differential analyzer study.

wide variety of velocity distributions, but it is believed that these distributions are representative of cases in which there are no marked nose-pressure peaks.

The water-drop-trajectory computations were made to encompass a speed range of 100 of 350 miles per hour (assuming incompressible flow), a drop-diameter range of 20 to 100 microns, and a variation in altitude from sea level to 20,000 feet. Airfoil chord length was varied from 3 inches to 30 feet. These variables were combined into the dimensionless parameters, ψ and R_V, which then were used as the independent variables throughout the trajectory computation. The range in values of ψ and R_V resulting from a combination of each minimum value and a combination of each maximum value of the three constituent variables is about 150 to 20,000 for ψ and about 35 to 1,000 for R_V. These ranges in ψ and R_V encompass most possible combinations of values of speed, drop size, altitude, and chord length.

The problem of obtaining area, rate, and distribution of water-drop impingement on an airfoil is one of determining the solution to a set of simultaneous differential equations yielding the trajectory or path which a water drop will follow. These equations, a derivation of which may be found in reference 6, are essentially those which result from imposing conditions of dynamic equilibrium on a drop moving in an air stream. In dimensionless form, the equations are

$$\frac{d(u_d/V)}{d\tau}=\frac{\psi}{R_V}\frac{C_dR}{24}\left(\frac{u_a}{V}-\frac{u_d}{V}\right) \tag{1}$$

$$\frac{d(v_d/V)}{d\tau}=\frac{\psi}{R_V}\frac{C_dR}{24}\left(\frac{v_a}{V}-\frac{v_d}{V}\right) \tag{2}$$

$$\left(\frac{R}{R_V}\right)^2=\left(\frac{u_a}{V}-\frac{u_d}{V}\right)^2+\left(\frac{v_d}{V}-\frac{v_d}{V}\right)^2 \tag{3}$$

Basically, equations (1) and (2) define the acceleration of a drop at any instant in orthogonal (x and y) directions. Consequently, a double integration of these equations, starting from a selected initial point (x_o, y_o), yields x and y coordinate values of a drop trajectory. Equation (3) is a simple identity used in the solutions of equations (1) and (2). In performing the integrations, knowledge of the quantity $C_dR/24$ (the ratio of the actual drag coefficient to that given by Stokes' law of resistance) is required; also required are magnitudes of the air-velocity components u_a/V and v_a/V as a function of drop location relative to the body. (See reference 6.) Variation of the term $C_dR/24$ with local Reynolds number R was taken from reference 7, while the variation of the air-velocity components u_a/V and v_a/V throughout the flow field was obtained analytically for the Joukowski airfoils. In the case of the NACA 65_2–015 airfoil, however, the velocity distribution throughout the flow field was obtained by an electrolytic analogy technique.[2]

In carrying out the differential analyzer computations for the five airfoil cases, the general procedure was to assign values to the terms ψ and R_V in equations (1), (2), and (3), to establish initial conditions, and then to obtain the water-drop-trajectory traces from the analyzer. For each combination of ψ and R_V selected, several trajectories were traced until the two trajectories were found, one for the upper surface and one for the lower surface, which were tangent to the airfoil surface at the point of drop impact. The importance of these two tangential trajectories lies in the fact that all drops between the tangential trajectories hit the airfoil and all drops outside will miss. In some cases, after the tangential trajectories were established, the distance between them was divided into six approximately equal spaces, and trajectories started at the boundary of each space were traced. These intermediate trajectories were used to obtain an indication of the distribution of water-drop impingement over the airfoil surface.

WATER-DROP TRAJECTORY DATA

In the water-drop-trajectory study, trajectories were calculated for assigned values of the independent variables ψ and R_V. These trajectories provided values of trajectory starting ordinates and surface positions of drop impingement from which values of the dependent variables, area, rate, and distribution of impingement, could be tabulated. A typical set of trajectories is shown in figure 2, and the numerical results obtained for the five airfoil cases are presented in tables I through V.

To obtain general trends from the water-drop-trajectory data, consideration was given to the desirability of developing a method for rapidly estimating values of area, rate, and distribution of impingement that would require only information which readily is obtainable for any airfoil profile. Airfoil contour and velocity distribution were taken as the information available for use in a design study. This report develops fairly simple and direct linking of the dependent variables, area, rate, and distribution of impingement, to airfoil contour and velocity distribution. The sequence in which airfoil contour and velocity distribution most readily are related to the dependent variables is as follows: (1) area, (2) rate, and (3) distribution of impingement. Development of the generalizations will be presented in this order.

TRENDS OBSERVED IN AREA OF WATER-DROP IMPINGEMENT DATA

In order to determine the area of water-drop impingement on the leading edge of an airfoil for specified meteorological and flight conditions, the values of s/c for the trajectories which impinge tangentially on the upper and lower surfaces must be obtained. In computational methods like those of references 3, 6, and 7, the procedure essentially has been to select values of ψ and R_V and then to determine the trajectory. Various trajectories are computed until the tangential trajectory for the upper and lower surfaces is found. The two tangential trajectories determine the farthest positions of drop impingement on the airfoil surface for the selected values of ψ and R_V and permit calculating area of impingement from the equation

$$A_s=\left[\left(\frac{s}{c}\right)_{u_t}-\left(\frac{s}{c}\right)_{l_t}\right]Lc$$

In the method derived in NACA TN 2476, the reverse procedure is employed; that is, a point on the airfoil is selected (s/c) and the corresponding ψ and R_V values which are associated with the tangential trajectories at that point are determined. The nature of the relationship between s/c and the parameters ψ and R_V is shown in figure 3. Data for the figure are those of table IV for the cambered airfoil at zero angle of attack and a lift coefficient of 0.44. From figure 3, it can be seen that any specified value of s/c in the figure can correspond to an infinite number of combinations of the variables R_V and ψ. Consequently, it becomes necessary to select values of two variables and to solve for the third. In the derivation of the procedure for estimating area of impingement, values of s/c and R_V are assumed and corresponding values of ψ are computed.

If, the data of figure 3 could be made available for all airfoils of interest, the problem of determining s/c for various values of ψ and R_V would not exist because the information obviously would be known. Because obtaining such data for all airfoils is impractical, the problem in the general case arises in determining values of ψ for given values of

[2] The technique of electrolytic analogy is based on the fact that the stream lines in an inviscid incompressible fluid and the equipotential lines in an electrical field are governed by the same equations. By means of this analogy and suitably constructed apparatus, velocities at any point in the flow field around a body can be measured directly.

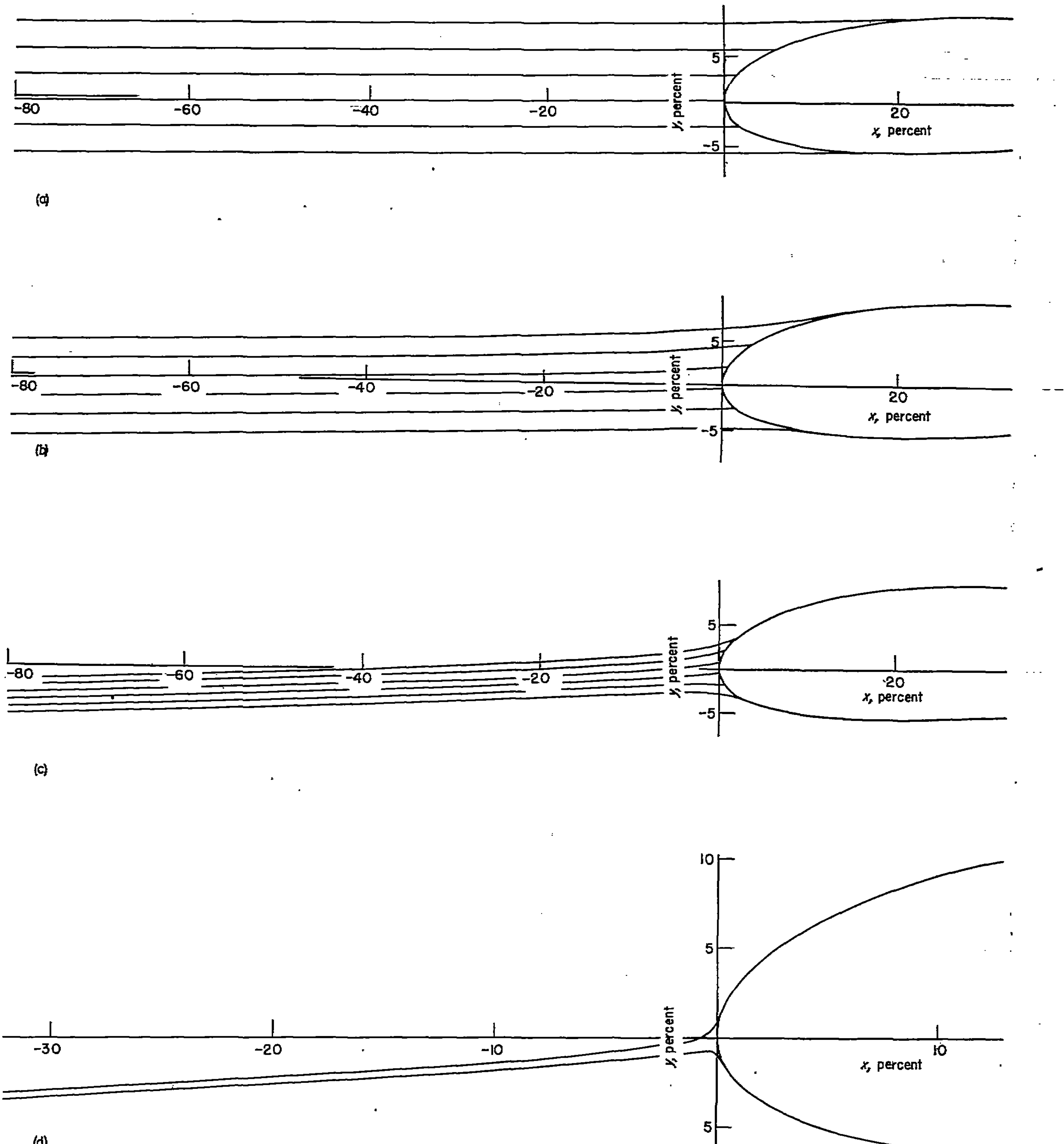

(a) $\psi=8$; $R_V=64$.
(b) $\psi=64$; $R_V=64$.
(c) $\psi=512$; $R_V=64$.
(d) $\psi=4096$; $R_V=64$.

FIGURE 2.—Typical water-drop trajectory traces from a differential analyzer; 15-percent-thick cambered Joukowski airfoil; $c_l=0.44$; $\alpha=0°$; $a=1.0$ mean line.

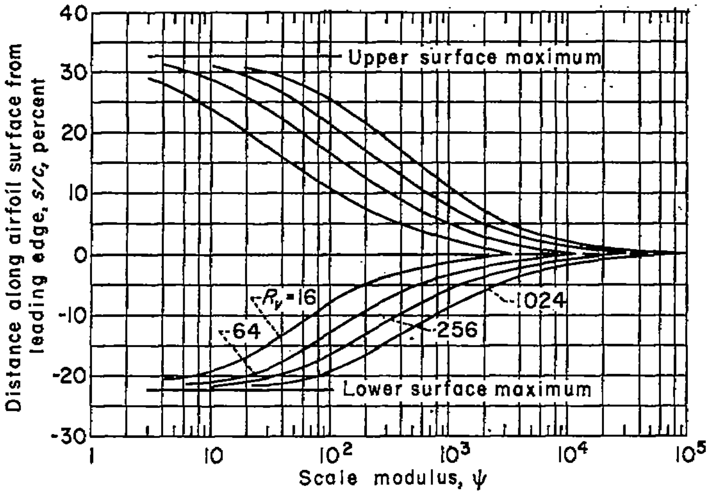

FIGURE 3.—Typical relation between farthest position of drop impingement, scale modulus, and free-stream drop Reynolds number; 15-percent-thick cambered Joukowski airfoil; c_l=0.44; α=0°; a=1.0 mean line.

s/c and R_V. To determine an expression for ψ, equations (1), (2), and (3) are utilized to give

$$\psi=\frac{a_d R_V}{\left(\frac{C_d R}{24}\right)\left(\frac{R}{R_V}\right)} \tag{4}$$

where

$$a_d=\sqrt{\left[\frac{d(u_d/V)}{d\tau}\right]^2+\left[\frac{d(v_d/V)}{d\tau}\right]^2}$$

Equation (4) expresses generally the relation between ψ and R_V at all points in a trajectory, and, therefore, it is applicable at the airfoil surface for an arbitrarily selected value of s/c which corresponds to some particular tangential trajectory. It remains to establish the values of $C_dR/24$, R/R_V, and a_d for the selected value of s/c. Actually, since $C_dR/24$ is a known function of R, the problem reduces to approximating R/R_V and a_d at the airfoil surface.

Evaluation of R/R$_V$ at airfoil surface.—To determine R/R_V the method of this report is based on a graphical solution utilizing the hodograph plane. A typical plot in the hodograph plane of the data from the differential analyzer is shown in figure 4 for the cambered Joukowski airfoil. To show the general relation of drop velocities to air velocities the hodograph of air at the airfoil surface is also shown in figure 4. Hodographs for the five airfoil cases, of which figure 4 is an example, revealed that the velocity components for all drops, regardless of the combination of ψ and R_V, can be represented by one faired curve. In addition, it became apparent that the hodograph for the drops, for both upper and lower airfoil surfaces, always passes through the point $u_d/V=\cos\alpha$, $v_d/V=\sin\alpha$. In the simplest case of an airfoil at zero angle of attack, the hodograph of the drops always passes through an abscissa value of unity since the point corresponds physically to the point of maximum airfoil thickness where the tangential trajectories are straight lines and impinge upon the airfoil with free-stream air velocity. The coordinates at the origin of the air and drop hodographs correspond, of course, to the airfoil stagnation point.

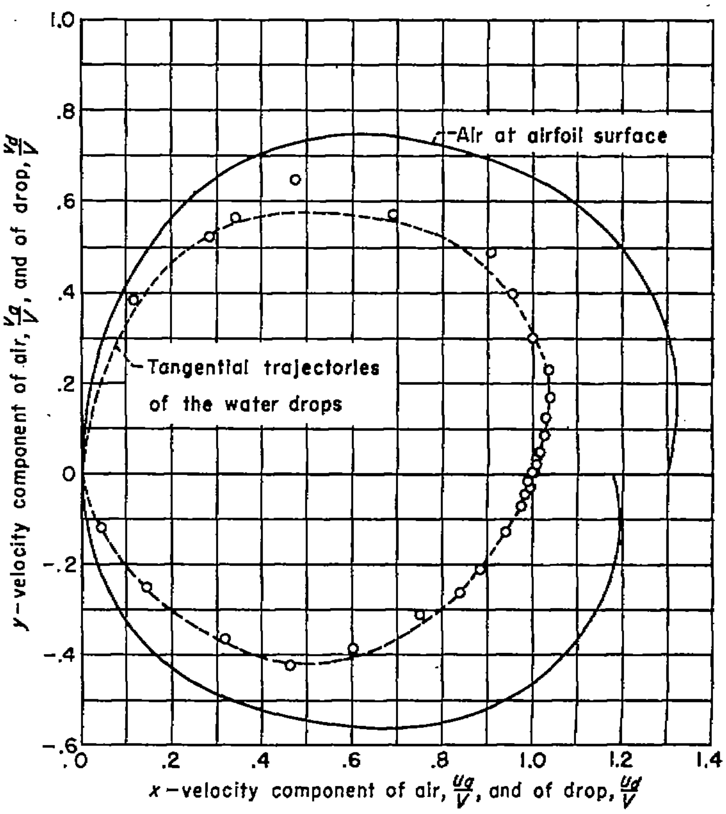

FIGURE 4.—Typical hodographs of tangential-trajectory velocities and air velocities on an airfoil surface; 15-percent-thick cambered Joukowski airfoil; c_l=0.44; α=0°; a=1.0 mean line.

To show the connection between the physical and hodograph planes, figure 5 is presented. Figure 5 (a) depicts several water-drop trajectories in the physical plane impinging tangentially at the same point s/c on an airfoil which is at an angle of attack α. For constant s/c (fig. 3) there are an infinite number of particular combinations of ψ and R_V which are affine to any particular position of tangential drop impingement $(s/c)_t$. In figure 5 (a), a single vector representing the drop velocity for all the trajectories is drawn tangentially to the airfoil at the point of drop impingement. Only one vector is shown because the tangential trajectory hodographs, such as that presented in figure 4, indicate that all drops impinging tangentially at a common point may be considered to have the same velocity. Also shown in figure 5 (a) is a vector representing the air velocity at the point of tangency for the trajectories. The angle between the drop- and air-velocity vectors and the x axis is designated by the angle θ. In figure 5 (b), a typical air and drop hodograph is shown and the same vectors as shown in the physical plane are indicated. The difference in length of air and drop vectors at a particular s/c position is numerically equal to the value of R/R_V given by equation (3). This equality provides a basis for predicting R/R_V, and forms the starting point for the empirical method.

Because an examination of the drop and air hodographs for the five airfoil cases showed that a single value of R/R_V can be considered to be associated with any particular s/c position, the assumption is made that other airfoils will display this same characteristic. In order to calculate values of R/R_V for an arbitrary airfoil, however, both hodographs of the air and of the tangential trajectories are required.

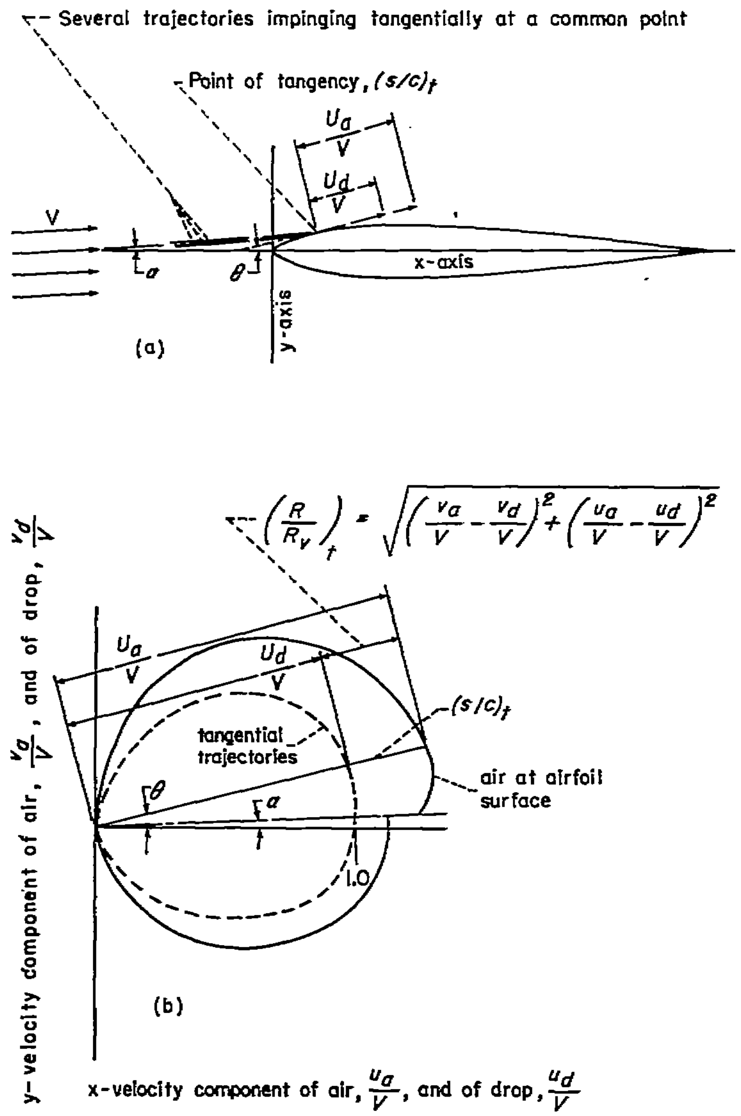

(a) Physical plane.
(b) Hodograph plane.

FIGURE 5.—Relationship between physical and hodograph planes for drop and air velocities at air foil surface.

The hodograph of the air velocity at the airfoil surface is easily obtained from the velocity distribution over the airfoil, so the problem is to determine the shape of the hodograph for the tangential trajectories. From physical considerations, it is known that the tangential-trajectory hodograph always will pass through the point $u_d/V=0$, $v_d/V=0$ and the point $u_d/V=\cos\alpha$, $v_d/V=\sin\alpha$.

With two points on the trajectory hodograph always known, it was postulated that, if one more point could be established, preferably where the vertical-velocity component reaches the maximum value, the general shape of the trajectory hodograph might be reasonably estimated. It was noted from the hodographs for the five airfoil cases that peak values of v_a/V and v_d/V were at nearly the same location on the airfoil surface; that is, values of $v_{a_{max}}/V$ and $v_{d_{max}}/V$ seem to fall on a straight line through the origin. A comparison was made, for the five airfoil cases, of values of the vertical component of relative velocity between drop and air attained at the position of maximum vertical air velocity. For this comparison, values of $(v_{a_{max}}/V)-(v_{d_{max}}/V)$ and $v_{a_{max}}/V$ were obtained from the five airfoil cases and these are plotted in figure 6. An inspection of the data in figure 6 shows that the four Joukowski airfoil cases provide a simple relation between $(v_{a_{max}}/V)-(v_{d_{max}}/V)$ and $v_{a_{max}}/V$. By use of figure 6, a third point on a trajectory hodograph can be ascertained which in turn permits the general shape of the hodograph to be estimated.

The point plotted in figure 6 for the NACA 65_2-015 airfoil upper surface does not lie on the curve established by the Joukowski airfoil data, and a question[3] arises as to whether this difference is real. While this question cannot be resolved until further data are available, qualitatively, it would seem that the tangential-drop velocities should tend to approach more nearly the surface-air velocities in the case of low-drag airfoils because these shapes are not so conducive to altering the paths or speed of water drops.

As an aid in discussing the construction of the drop hodograph using only three points, figure 7 is presented. In figure 7 the air hodograph is first drawn, and the point $v_{a_{max}}/V$ is established. Then, of the three methods considered, one procedure to obtain a drop hodograph uses the maximum vertical velocity of the tangential-trajectory hodograph $v_{d_{max}}/V$. This value is determined as being less than $v_{a_{max}}/V$ by the amount $(v_{a_{max}}/V)-(v_{d_{max}}/V)$ in accordance with the curve in figure 6. The value of $v_{d_{max}}/V$ so determined is assumed to lie on a straight line connecting the origin and $v_{a_{max}}/V$. The position of $v_{d_{max}}/V$ along the radial line determines the value of $(R/R_V)_{v_{a_{max}}}$ at that particular position. Values of R/R_V for other s/c positions might be taken, as a first approximation, as being in the same ratio to the air velocity at the particular s/c position as the value of R/R_V at $v_{a_{max}}/V$ is to U_a/V at $v_{a_{max}}/V$ (curve A in fig. 7). Thus, an expression for R/R_V at an s/c position would be:

$$\frac{R}{R_V}=\frac{U_a}{V}\times\frac{(R/R_V)_{v_{a_{max}}}}{(U_a/V)_{v_{a_{max}}}} \tag{5}$$

Values of R/R_V calculated by equation (5) usually are too large near point X (fig. 7) where it is known that $u_d/V=\cos\alpha$, $v_d/V=\sin\alpha$, so that a drop hodograph so constructed probably would not pass through this point, and it should. To overcome this discrepancy in the drop hodograph as computed, assuming a constant value of $\frac{R/R_V}{U_a/V}$ based on the peak point of the air hodograph, a curve without reflex is faired tangentially into this drop hodograph from the point $u_d/V=\cos\alpha$, $v_d/V=\sin\alpha$. The combination of the proportional curve and the faired curve comprises the drop hodograph, which is labeled curve B in figure 7. For the five airfoil cases maximum deviations between the drop hodographs obtained by the foregoing method and actual drop hodographs were of the order of 15 percent in the value of U_d/V.

Two other methods were considered for establishing drop hodographs. One of these methods assumed R/R_V to main-

[3] Some variation in the value $(v_a/V)_{max}-(v_d/V)_{max}$ can be obtained by the choice of curve used for the drop hodograph. In the case of the NACA 65_2-015 airfoil, the latitude of choice for a hodograph was fairly great because of some discrepancies in the velocity-component data corresponding to small values of s/c. The hodograph finally chosen, and which gives rise to the questioned point in figure 6, is based only on the most reliable velocity-component values from the data.

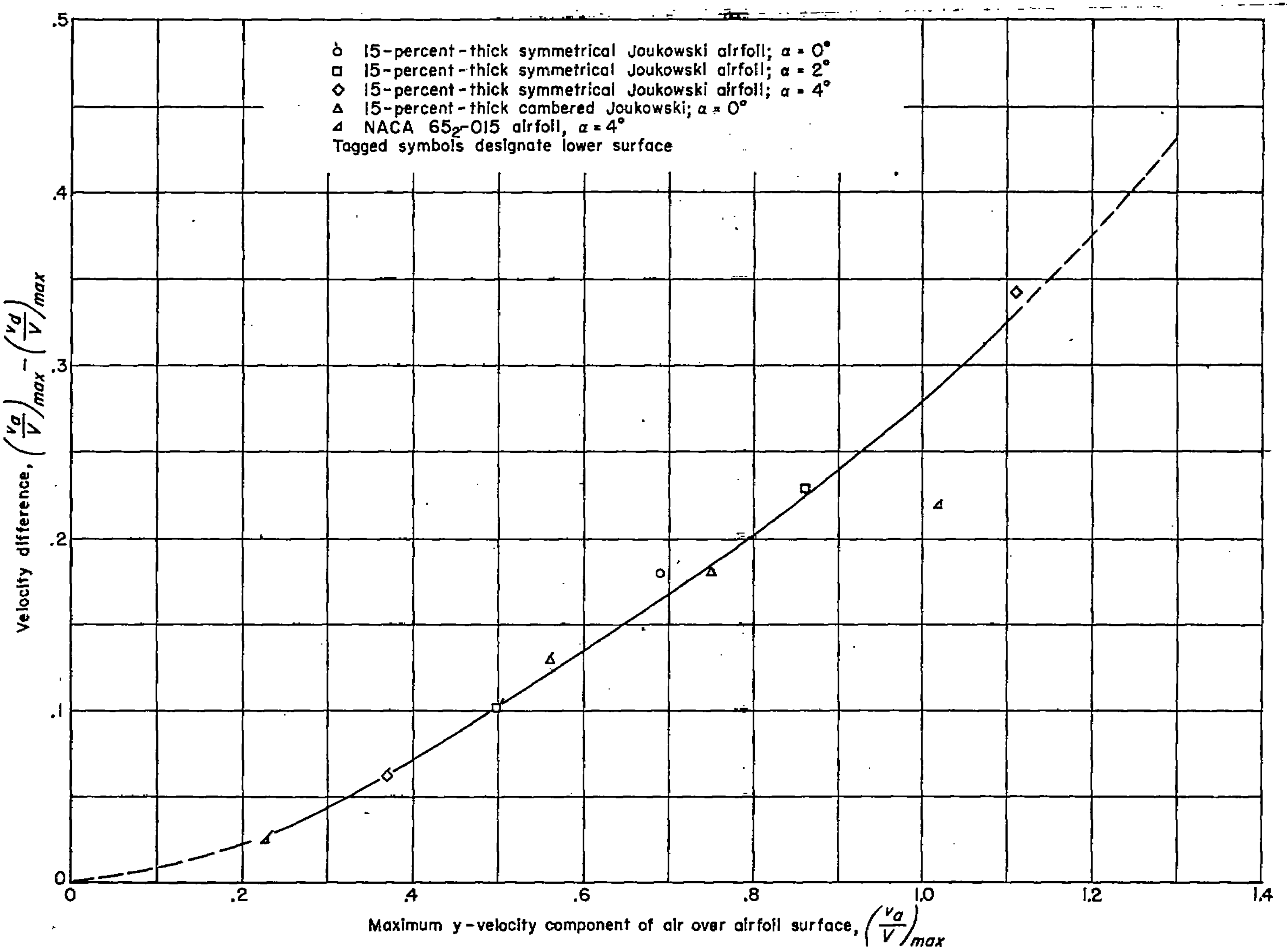

FIGURE 6.—Variation of velocity difference between drop and air with maximum y-velocity component of air for the five airfoil cases investigated.

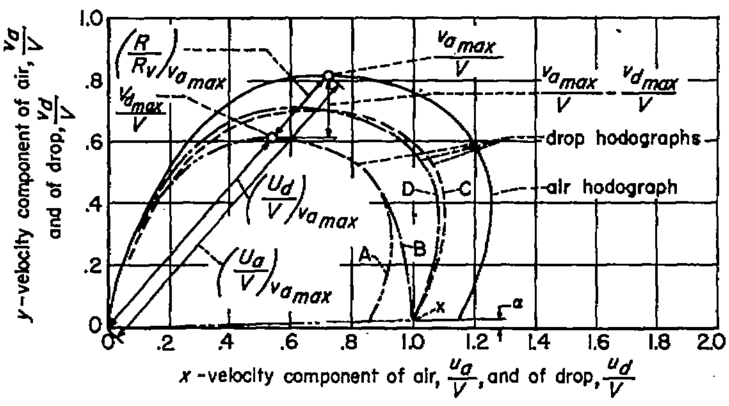

Curve A based on $\frac{R}{R_V}=\left(\frac{R}{R_V}\right)_{v_{a_{max}}}\times\frac{(U_a/V)}{(U_a/V)_{v_{a_{max}}}}$
Curve B faired tangentially to curve A from point X.
Curve C based on (R/R_V)=constant.
Curve D based on $\frac{(R/R_V)}{(U_a/V)}$=constant.

FIGURE 7.—Illustration of three possible techniques for the construction of a drop hodograph from a specified air hodograph.

tain a constant value equal to the value prevailing at the point $u_d/V=\cos\alpha$, $v_d/V=\sin\alpha$. The other method assumed the ratio $\frac{R/R_V}{U_a/V}$ to maintain a constant value determined by the value of R/R_V and U_a/V at the point $u_d/V=\cos\alpha$, $v_d/V=\sin\alpha$. The drop hodographs given by each of these two methods also are shown for the example in figure 7. The curves are labeled C and D, respectively. These two methods have the advantage of not requiring the use of the hodograph and figure 6; however, they are considerably more inaccurate (maximum deviations from the drop hodographs for the five airfoil cases being in the order of 30 percent), due to the neglect of factors of apparent influence on the drop trajectories. Either one of these latter two methods might be useful for particular airfoil cases which happen to fall considerably beyond the scope of the data used to obtain figure 6.

After the tangential-trajectory hodograph has been established in relation to the hodograph for air, values of R/R_V are available for various chordwise positions on the airfoil. These values are used in equation (4) for arbitrarily selected values of R_V and s/c. Once values of R_V are selected, values of R are ascertainable. Furthermore, the term $C_dR/24$ is the function of R tabulated in table VI. Thus, to solve equation (4), the only additional term to be evaluated is a_d.

Evaluation of the drop-acceleration term a_d.—The remaining term to be evaluated in equation (4) is the acceleration of the drop at the airfoil surface a_d. To determine the variation of this term with chordwise position, values of a_d were calculated from the trajectory data by equation (4) for each of the airfoil cases presented in tables I through V. The procedure used in making the calculations was to compute the value of R/R_V by utilizing values of the orthogonal drop-velocity components from tables I through V for corresponding values of ψ and R_V. The term was calculable through knowledge of R/R_V and R_V. The terms R/R_V, $C_dR/24$, R_V, and ψ were then substituted into equation (4) and solved for a_d. The results for a typical case (15-percent-thick cambered Joukowski airfoil) are presented in figure 8.

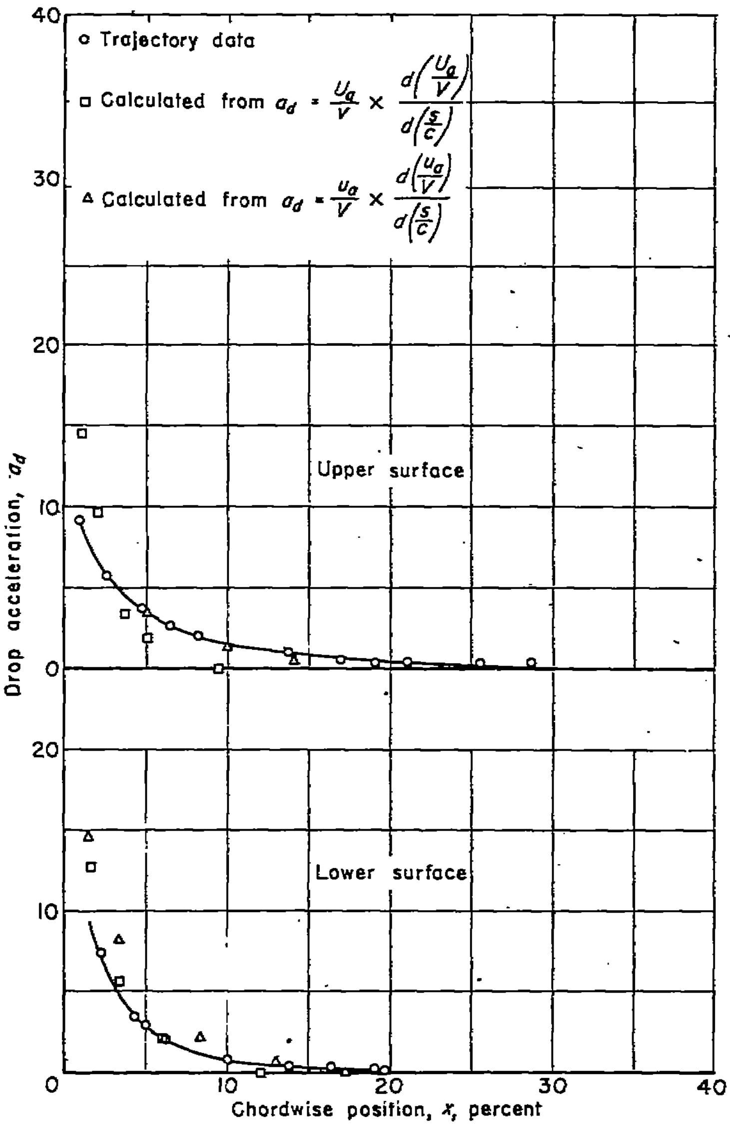

FIGURE 8.—Typical chordwise distribution of instantaneous drop-acceleration values, for tangential trajectories at instant of drop impact; 15-percent-thick cambered Joukowski airfoil; $c_l=0.44$; $\alpha=0°$; $a=1.0$ mean line.

Figure 8 exemplifies that drop acceleration at the surface of the airfoil, like the hodograph of drop velocities for tangentially impinging trajectories, can be considered a single relation regardless of the combinations of ψ and R_V. How the singular nature of the acceleration values arises can be shown as follows:

Equation (4) may be written

$$a_d=\psi\left(\frac{C_d}{24}\right)\left(\frac{R}{R_V}\right)^2_t \tag{6}$$

However, since the term $(R/R_V)_t$ is taken to be constant for a given position on the surface, equation (6) may be written, for any given chordwise position,

$$a_d=(\text{const})\ \psi C_d \tag{7}$$

Thus, according to equation (7), if the product of ψ and C_d remains constant for various values of R_V at a given chordwise position, then the value of a_d also will remain constant. Comparisons were made, for the five airfoil cases, of $\psi\ C_d$ products for given s/c positions over a wide range in ψ and R_V values. These comparisons showed that, for a given s/c position, the product of ψ and C_d generally is of similar magnitude. A sample of such a comparison for the 15-percent-thick cambered Joukowski airfoil at 0° angle of attack is shown in table B in which values of ψ, for chosen values of R_V and s/c, were taken from curves faired from the data tabulated in table IV. On the basis of comparisons of ψC_d products for the five airfoil cases, the assumption that a_d is constant for a particular chordwise position seems fairly well justified.

TABLE B.—COMPARISON OF PRODUCTS OF SCALE MODULUS AND DROP DRAG COEFFICIENT FOR A 15-PERCENT-THICK CAMBERED JOUKOWSKI AIRFOIL

[$\alpha=0°$; $c_l=0.44$; $a=1.0$ mean line]

	ψC_d			
	Upper surface			
s/c \ R_V	16	64	256	1024
25.0	62	65	65	66
20.0	152	165	166	164
15.0	345	348	337	346
10.0	877	885	880	830
5.0	3500	3110	2742	2600
2.5	8950	7677	6630	6590
	Lower surface			
−20.0	65	67	55	63
−15.0	271	234	204	204
−10.0	547	510	492	478
−5.0	1620	1640	1698	1741
−2.5	5800	5400	5850	5920

After inferring that the value of a_d can be considered as being unique at any particular chordwise position, regardless of the values of ψ and R_V, the problem of evaluating drop acceleration becomes one of determining the appropriate value of a_d to assign to each value of s/c.

In approximating the drop acceleration at a point where the drop trajectory is tangent to the airfoil surface, several procedures were tested, as was the case with the term R/R_V. Of the various procedures investigated, the one which will be presented herein is considered most acceptable because the resultant accuracy is commensurate with that produced by the most accurate procedure presented for obtaining R/R_V. In addition, the procedure is simple in application.

For this procedure, the approximation is made that the tangential acceleration of a drop at a given point on the surface is the same as the acceleration of the air along the airfoil surface at the same point.[4] The equation used to express the drop acceleration in terms of air velocity at the airfoil surface is:

$$a_d = \frac{U_a}{V} \times \frac{d(U_a/V)}{d(s/c)} \qquad (8)$$

The velocity-gradient term in equation (8) can be evaluated simply by plotting U_a/V against s/c, and obtaining the slope of the curve at the desired s/c positions.

Results typical of those obtained by using equation (8) to approximate values of a_d are shown in figure 8 for the cambered Joukowski airfoil. The calculated points are denoted by square symbols. Figure 8 illustrates the general finding that equation (8) provides over most of the airfoil lower surface values of a_d which are in good agreement with the data. On the airfoil upper surface, equation (8) provides drop-acceleration values which are in fair agreement with the data near the airfoil leading edge; but farther aft, the ability of equation (8) to predict appropriate values diminishes appreciably. This decrease in accuracy was most pronounced for the Joukowski and NACA 65_2–015 airfoils at 4° angle of attack. For the two 4° angle-of-attack cases, the inability of equation (8) to represent actual drop acceleration values fairly far aft on the airfoil surface apparently is because the drops impinging in this region have sufficiently large inertia so as not to respond to the very rapid changes in surface-air velocities prevailing near the position of maximum air velocity. Except quite near the leading edge, the trajectories are fairly straight, indicating that the impinging drops do not respond appreciably to the vertical components of air velocity. Thus, another approximation of drop acceleration can be obtained by using the x components of air velocity. In equation (8), U_a/V would be replaced by u_a/V so that

$$a_d = \frac{u_a}{V} \times \frac{d(u_a/V)}{d(s/c)} \qquad (9)$$

Results obtained by using equation (9) are presented in figure 8 using the cambered Joukowski airfoil as a representative illustration. The values calculated by equation (9) are shown in the figure by triangular symbols. For the airfoil upper surface, the agreement between calculated values and trajectory data is good fairly far aft on the airfoil; on the lower surface, the agreement also appears to be reasonably good. Apparently then, equation (9) can be helpful when estimating a_d values for airfoils at angle of attack.

The question arises as to whether it would be possible in the general case, when the differential analyzer data points shown in figure 8 were not present, to detect the inadequacy of equations (8) or (9) to represent the correct values of a_d. In this regard, it should be noted that s/c values for $a_d=0$ always can be selected because these values correspond to chordwise positions of tangentially impinging straight-line trajectories having maximum s/c intercept. These particular trajectories always can be established by constructing lines tangent to the upper and lower surfaces of the airfoil parallel to the free-stream direction. With s/c values for $a_d=0$ established, there would be some indication of when these equations could not truly represent the correct curve. Because, for an arbitrary airfoil case, there is no absolute assurance that either equation (8) or equation (9) will provide values of a_d which will represent the correct curve, it is suggested that both equations be employed in estimating values. If, in using equations (8) and (9), the value of s/c for which $a_d=0$ is found to differ materially from the value given by straight-line trajectories impinging tangentially on the airfoil, then the calculated values should be regarded with some skepticism. In such an event, reliance should be placed mostly on the values of a_d calculated by equation (8) for small s/c values, and a curve faired from these values to a value of zero acceleration at the known extreme position of drop impingement.

Calculation of scale modulus ψ for s/c at the stagnation point.—The two preceding subsections have presented approximate methods by means of which equation (4) can be evaluated to obtain values of ψ for selected R_V values at chosen positions on the airfoil surface. However, a special procedure for evaluating ψ at the stagnation point is necessary, since equation (4) cannot be used to evaluate the scale modulus at or very near the stagnation point. This procedure is more suitably discussed in connection with the section on rate of impingement which follows:

TRENDS OBSERVED IN RATE-OF-IMPINGEMENT DATA

Another quantity of interest to the designer of an aircraft thermal-ice-prevention system is weight rate of drop impingement on an airfoil. An expression for weight rate of drop impingement per unit length of span, according to reference 8, is given by

$$M_t = 3600\, Vm\Delta y_o{}'_t \qquad (10)$$

In order to evaluate the rate of impingement M_t in accordance with equation (10), the term $\Delta y_o{}'_t$ must be known. When methods like those of references 3, 6, and 7 are employed, $\Delta y_o{}'_t$ can be determined directly from the calculated trajectories which impinge tangentially upon the airfoil. For a procedure in which trajectories themselves are not determined, however, evaluation of $\Delta y_o{}'_t$ must be based upon quantities which are known.

Evaluation of $\Delta y_o{}'_t$ using airfoil ordinates as an intermediate parameter.—Preceding sections have shown that $(s/c)_{u_t}$ and $(s/c)_{l_t}$ can be established as a function of ψ for various values of R_V; hence, the airfoil ordinates corresponding to the farthest position of drop impingement on the upper and lower surfaces y_{u_t} and y_{l_t} also can be ascertained as a function of ψ for various values of R_V. Because values of y_{u_t} and y_{l_t} can be obtained readily for a wide range of ψ and R_V values, the data were examined for a relationship involving Δy_{o_t} (for small angles of attack, Δy_{o_t} is approximately equal to y_{o_t},) and the quantity $y_{u_t}-y_{l_t}$ which will be called

[4] Only the tangential component of drop acceleration needs to be approximated since the normal component of drop acceleration is equal to zero at the point of tangency. That the normal acceleration of the drop is zero at this point can be shown by writing the equations expressing dynamic equilibrium of a drop. The terms involving the drop and air velocities are resolved normally and tangentially. A substitution of the boundary conditions at this point shows that the normal acceleration must equal zero.

Δy_t. In this regard, Δy_{o_t} was compared with Δy_t for the values of ψ and R_V values presented in tables I through V for the five airfoil cases. Results typical of the comparisons for the five airfoil cases are shown in figure 9 for the 15-percent-thick cambered Joukowski airfoil at 0° angle of attack:

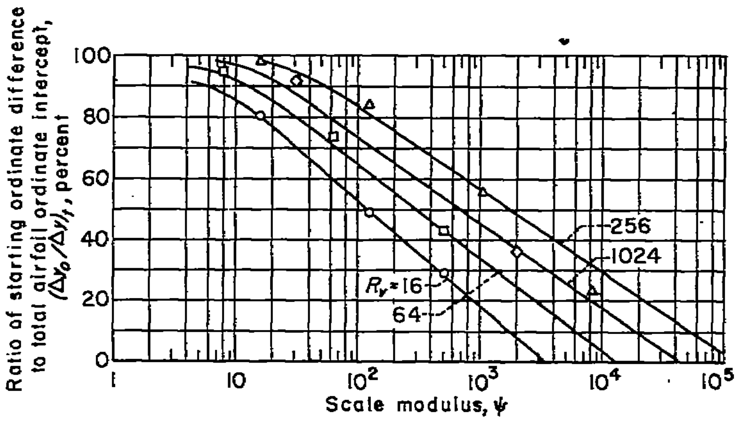

FIGURE 9.—Typical variation of the ratio of trajectory starting ordinate difference to total airfoil ordinate intercept as a function of scale modulus and free-stream Reynolds number; 15-percent-thick cambered Joukowski airfoil; c_l=0.44; α=0°; a=1.0 mean line.

An inspection of data for the five cases showed that the ratio of Δy_{o_t} to Δy_t can be considered linear with respect to the log of the scale modulus ψ for various R_V values. The linearity was found to exist for values of $(\Delta y_o/\Delta y)_t \leq 0.8$ for the Joukowski airfoils, and for values of $(\Delta y_o/\Delta y)_t \leq 0.9$ for the NACA 65_2–015 airfoil; but this linearity appears to be characteristic only of airfoils since cylinder data from reference 7, when plotted in the same manner do not show this property. Of special interest in figure 9, however, is the fact that the ratio $(\Delta y_o/\Delta y)_t$ must become zero at some particular value of ψ for a given value of R_V. This "critical" value of ψ can be calculated from an aerodynamic property of the airfoil. According to references 7 and 9, for symmetrical bodies at 0° angle of attack, the critical value of ψ (i. e., the maximum value for a given value of R_V for which drops just impinge on the body) is given by

$$\psi_{cr}=4R_V\frac{\partial(u_a/V)}{\partial x}\bigg|_{\Psi=0} \tag{11}$$

For symmetrical bodies at an attitude other than 0°, or for unsymmetrical bodies at an arbitrary attitude, the same form of equation (11) applies, but with the notation slightly altered; thus,

$$\psi_{cr}=4R_V\frac{\partial(U_a/V)}{\partial S}\bigg|_{\Psi=0} \tag{12}$$

This change is made because the small drop which impinges only at the stagnation point of the airfoil follows the stagnation streamline which, in the general case, is not a line parallel to the airfoil chord line. For simplicity, equation (12) shall be written

$$\psi_{cr}=4R_VG \tag{13}$$

In order to use equation (13), the problem of assigning a value of G presents itself for the case of an arbitrary airfoil. Since the quantities s/c and E are affected only in a minor way by variations in G,[5] it was believed that for determining G the airfoil could be replaced by a shape more amenable to calculation. The assumption was made that a symmetrical Joukowski airfoil would be representative of that type section having maximum thickness fairly well forward (conventional airfoils), and an ellipse representative of that type section having maximum thickness well aft (low-drag airfoils). Since the major factors influencing the value of G are thickness and angle of attack, calculations of G were made for symmetrical Joukowski airfoils and ellipses of different thickness-chord ratios at various lift coefficients.[6] The results of these calculations are presented in figure 10. The data in figure 10 (a) are intended for use with airfoils resembling Joukowski airfoils and may be used directly. The data in

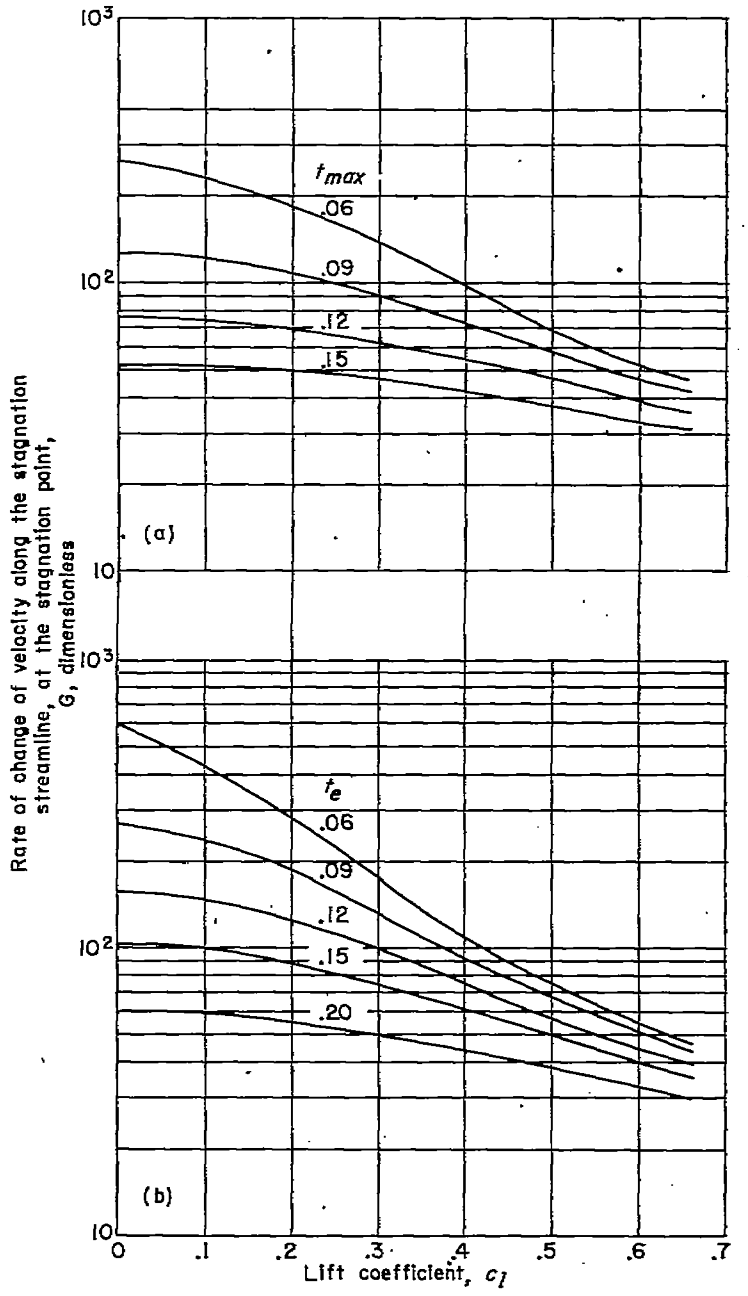

(a) Joukowski airfoil.
(b) Ellipse.

FIGURE 10.—Velocity gradient along the stagnation streamline at the stagnation point, as a function of lift coefficient and thickness ratio for two profiles.

[5] Calculations have shown that negligible changes in s/c and E occur for a change in G as large as 10 percent.

[6] No account is taken of the effect of a cambered profile on the velocity gradient G. The reason for neglecting this effect is that tests using an electrolytic analogy have shown that the effects of camber are very small in comparison with the effects of thickness, and calculations have shown that only large variations in G are important in affecting the values of s/c and E

figure 10 (b) are intended for use with low-drag profiles; however, it is first necessary to establish an "equivalent ellipse" thickness ratio for the low-drag section being used. An equivalent ellipse is defined for the purposes of figure 10 (b) as an ellipse having its leading-edge radius equal to the leading-edge radius of the airfoil, and a thickness equal to the airfoil maximum thickness. The major axis of the ellipse is thus established and the ellipse thickness ratio can be computed. An equation expressing the thickness ratio of the equivalent ellipse in terms of the airfoil leading-edge radius and thickness ratio is:

$$t_e=\frac{2\rho}{t_{max}} \tag{14}$$

With the aid of figure 10, the value of ψ_{cr} for airfoils can be estimated for any R_V value in accordance with equation (13). Not only does this value correspond to the condition of zero rate of impingement, but it also corresponds to the condition of zero area of impingement. Hence, the critical value of ψ can be used for obtaining an additional point for area-of-impingement computations, and this value will correspond to the s/c value at the stagnation point.

While the condition of no drops impinging on the airfoil surface yields one point on the curves, $(\Delta y_o/\Delta y)_t$ versus log ψ, at least one more point is required for each value of R_V in order to establish the linear relationships as observed in figure 9. To locate a second point on an isopleth of R_V, it is desirable to determine a value of ψ corresponding to a chosen value of $(\Delta y_o/\Delta y)_t$ somewhat less than unity. The reason for this specification is to procure a spread in the values of $(\Delta y_o/\Delta y)_t$ used to establish the linear relationships, between $(\Delta y_o/\Delta y)_t$ and log ψ, for isopleths of R_V.

In developing a procedure for determining what value of ψ is associated with a specified value of $(\Delta y_o/\Delta y)_t$ on an isopleth of R_V, the data from the five airfoil cases were examined for values of some parameter, related to $(s/c)_{u_t}$ and $(s/c)_{l_t}$, which could be used to fix the value of ψ. The parameter used to supply the necessary values was the efficiency of drop impingement E. The relationship between E and $(\Delta y_o/\Delta y)_t$ is given by

$$E=\left(\frac{\Delta y_o}{\Delta y}\right)_t\left(\frac{\Delta y_t}{t_{max}}\right) \tag{15}$$

Equation (15) can be derived by starting from the definition of E in terms of the initial drop-trajectory ordinates

$$E=\frac{(y_{o_u}{}'-y_{o_l}{}')_t}{h}=\frac{\Delta y_{o_t}{}'}{h} \tag{16}$$

At the small angles of attack associated with most flight conditions, $\Delta y_{o_t}{}'$ in equation (16) can be replaced by Δy_{o_t} so that

$$\Delta y_{o_t}=Eh \tag{17}$$

Then, in equation (17), if the reference dimension h is replaced by t_{max} and both sides of equation (17) are divided by Δy_t, and the terms rearranged, equation (15) is obtained.

The trajectory data for the five airfoil cases provided, for different values of R_V, relatively constant values of E corresponding to a value[7] of $(\Delta y_o/\Delta y)_t=0.8$. These efficiency values were used to obtain an average efficiency value for each airfoil case. Then, by using equation (15), an average value of $\Delta y_t/t_{max}$ could be computed for each airfoil case by using the average efficiency values and a value of $(\Delta y_o/\Delta y)_t=0.8$. The results are presented in table C.

TABLE C.—AVERAGE VALUES OF $\Delta y_t/t_{max}$ OBTAINED FROM EFFICIENCY DATA FOR THE FIVE AIRFOIL CASES AT A VALUE OF $(\Delta y_o/\Delta y)_t=0.8$

Case number	Efficiency of impingement, E (percent)									$\frac{\Delta y_t}{t_{max}}$
	R_V								Average value for each case	
	16	32	64	128	256	512	1024	2048		
1	----	77.5	----	77.0	----	75.5	----	78.0	77.0	0.96
2	76.0	----	74.5	----	75.5	----	77.5	----	75.8	.95
3	72.0	----	73.0	----	72.0	----	70.5	----	71.8	.90
4	77.0	----	82.0	----	86.0	----	82.0	----	81.7	1.02
5	55.0	----	59.0	----	56.5	----	55.0	----	56.4	.71

The values of $\Delta y_t/t_{max}$ tabulated in table C exhibit some variation between airfoil cases, and figure 11 is presented to show this variation when $\Delta y_t/t_{max}$ is assumed to be a function only of angle of attack. In figure 11, the point for the NACA 65_2-015 airfoil does not lie on the curve presented for the Joukowski airfoils. If the variation of $\Delta y_t/t_{max}$ with angle of attack shown in figure 11 is used, it is possible to

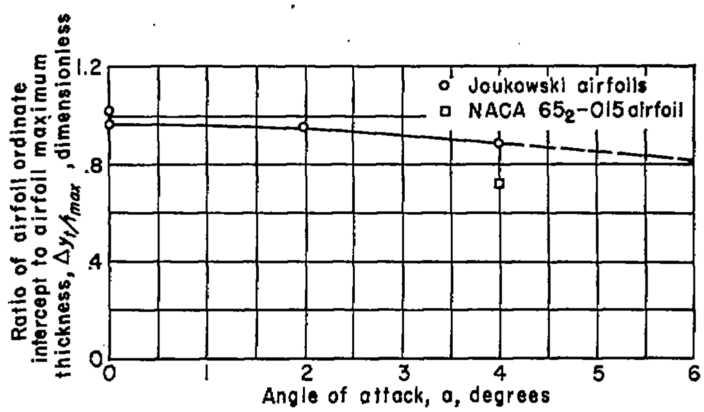

FIGURE 11.—Ratio of $\Delta y_t/t_{max}$ as a function of angle of attack for $(\Delta y_o/\Delta y_t)=0.8$.

determine, for a given value of R_V, an approximate value of ψ at which $(\Delta y_o/\Delta y)_t=0.8$. The procedure which may be used for determining this value of ψ is shown by a hypothetical example in figure 12. From curves of $(s/c)_{u_t}$ and $(s/c)_{l_t}$ as a function of log ψ for a specified value of R_V (fig. 12 (a)), curves of y_{u_t} and y_{l_t} as a function of log ψ are established for the same value of R_V (fig. 12 (b)). For the relation shown in figure 12 (b), there is a value of $\Delta y_t/t_{max}$ which is the same as would be chosen from the relation in figure 11 corresponding to the airfoil angle of attack. This particular value of $\Delta y_t/t_{max}$ corresponds to the ψ value at which $(\Delta y_o/\Delta y)_t=0.8$ for the particular R_V value chosen (fig. 12 (c)), and the

[7] The procedure utilized was to determine from curves of $(\Delta y_o/\Delta y)_t$ as a function of log ψ (fig. 9) the value of ψ at which $(\Delta y_o/\Delta y)_t=0.8$ for different values of R_V. Then, data from tables I through V were used to establish curves of E as a function of log ψ for the same values of R_V. On the efficiency curves, the value of E corresponding to $(\Delta y_o/\Delta y)_t=0.8$ for a particular value of R_V could be determined by locating, for the same R_V value, the value of ψ which was established from curves, similar to that in figure 9, to correspond to $(\Delta y_o/\Delta y)_t=0.8$.

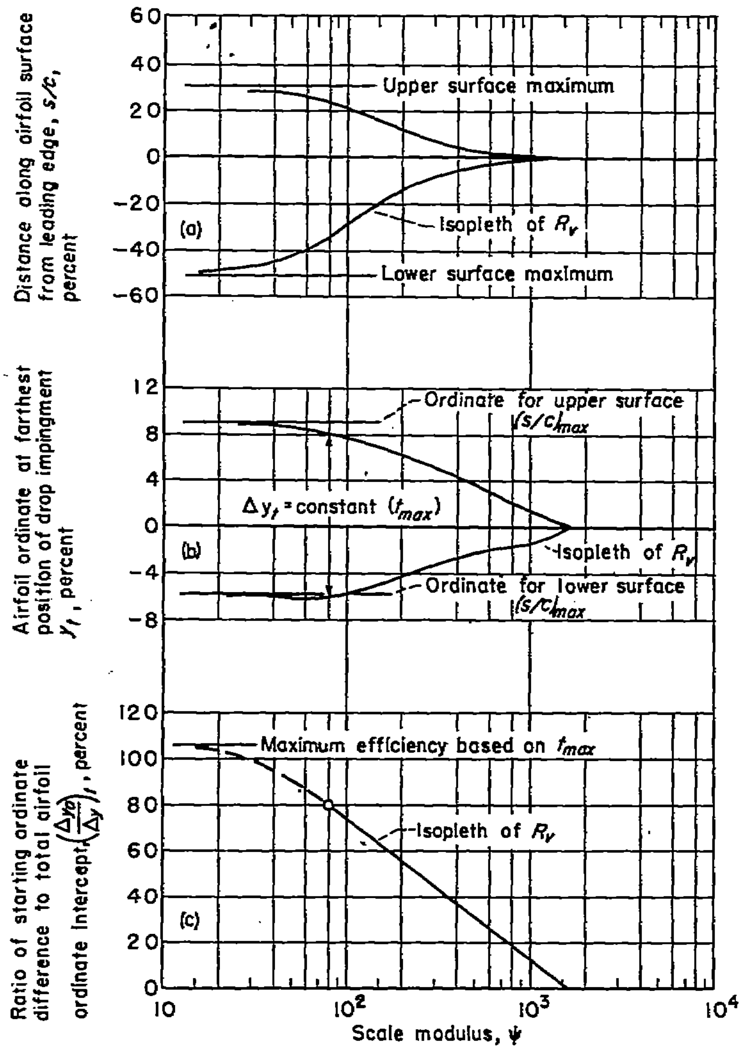

(a) Farthest position of drop impingement.
(b) Airfoil ordinate at farthest position of drop impingement.
(c) Ordinate-intercept ratio.

FIGURE 12.—Graphical representation of the procedure used to obtain a value of ψ corresponding to $(\Delta y_0/\Delta y)_t=0.8$

second point on an isopleth of R_V for $(\Delta y_o/\Delta y)_t$ as a function of log ψ is thereby determined.

The previous discussion has shown how values of Δy_{o_t} may be obtained for various ψ and R_V values. However, in the design of a thermal ice-protection system, by the method discussed in reference 1, it is sometimes more convenient to determine the rate of water-drop impingement by using the airfoil collection efficiency E rather than by using the term $\Delta y_{o_t}'$. In such circumstances, equation (10) becomes

$$M_s=3600\,VmEt_{max}$$

wherein E would be given by equation (15). When equation (15) is used and the angle of attack is other than zero, the limit efficiency value corresponding to straight-line trajectories will be greater than unity because h usually is somewhat greater than t_{max}.

TRENDS OBSERVED IN DISTRIBUTION OF IMPINGEMENT DATA

Of secondary importance in the design of heated wings is distribution of water-drop impingement over the length of interception along the airfoil surface. Despite its lack in prime importance, information concerning distribution of water drops over an airfoil sometimes is desired and, therefore, brief mention shall be made of observations drawn from the differential analyzer results.

An examination of the trajectory data did not reveal any direct empirical way to obtain a functional relation between impingement distribution, scale modulus, and free-stream-drop Reynolds number. It was found, however, that a graphical construction can be used to approximate the distribution of drop impingement over an airfoil surface. The basis for the graphical procedure was found by examining the variation of the concentration factor [8] C as a function of s/c for various combinations of ψ and R_V. Two such variations, which are typical of the five airfoil cases investigated, are presented in figure 13 for a 15-percent-thick cambered Joukowski airfoil at 0° angle of attack. The

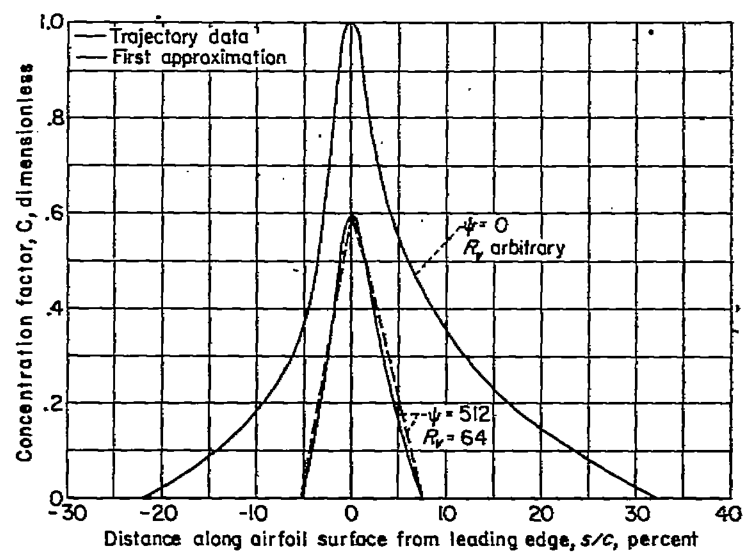

FIGURE 13.—Surface distribution of water-drop impingement for a 15-percent-thick cambered Joukowski airfoil; c_l=0.44; α=0°; a=1.0 mean line.

curves depicting these variations in figure 13 are shown by solid lines. One curve is typical for combinations of ψ and R_V corresponding to curved trajectories, and the other curve is typical for the combination of ψ and R_V corresponding to straight-line trajectories (ψ=0, value of R_V arbitrary). The curve for ψ=0 is obtained by drawing a number of straight-line trajectories to the airfoil to obtain values of the concentration factor

$$C=\frac{dA_o}{dA_s} \qquad (18)$$

and represents the locus of maximum possible values of C. This curve, which will be referred to as a limit curve, always can be obtained for a given airfoil because straight-line trajectories always can be reproduced, but the curve for values of C less than maximum cannot be obtained because the shape of the curved trajectories cannot be determined. Because of the shape of the C distribution curves noted for the five airfoil cases, and of which figure 13 is an example, a triangular distribution is considered useful in establishing a first approximation to an actual distribution. For a tri-

[8] The use of the concentration factor C in the computation of heat requirement due to drop impingement is discussed in reference 1.

angular distribution, the maximum value of C can be calculated from the equation

$$C_{max}=\frac{Eh}{(s_{av})_t} \qquad (19)$$

which is developed in NACA TN 2476. The value of C_{max} given by equation (19) is considered to lie on a line connecting the points $C=1.0$, $s/c=0$, and $C=0$, and s/c for the stagnation point. The values of $(s/c)_{u_t}$ and $(s/c)_{l_t}$ are used to define the extremities of the triangular distribution for a value of $C=0$. An example triangular distribution is shown in figure 13 for the 15-percent-thick cambered Joukowski airfoil at 0° angle of attack. The distribution is constructed corresponding to values of $\psi=512$ and $R_V=64$ and is compared in the figure to the distribution given by the trajectory data for the same values of ψ and R_V.

The value of C_{max} obtained from equation (19) always will be low. However, if the triangular approximation is altered to correspond more nearly to the shape of the limit curve for the C values, while keeping the enclosed area the same as the triangular area, more accurate concentration-factor values can be obtained. The altering of the triangular distribution is an attempt to establish the locus of concentration-factor values which would be given by data for calculated trajectories.

A PROCEDURE FOR CALCULATING AREA, RATE, AND DISTRIBUTION OF WATER-DROP IMPINGEMENT ON AN ARBITRARY AIRFOIL

Previous sections have shown how trends derived from the water-drop trajectory data may be applied to determine area, rate, and distribution of impingement for an arbitrary airfoil in incompressible flow. The general procedure will now be summarized by using, as an example, the case of an NACA 23015 airfoil at $c_l=0.5$.

AREA OF IMPINGEMENT

The procedure for calculating area of impingement consists primarily in determining values of $(s/c)_{u_t}$ and $(s/c)_{l_t}$. The following steps explain how the empirical relations derived from the trajectory data could be used to determine these values, and figure 14 incorporates necessary accompanying graphical relationships:

Step 1.—Construct the following curves for use during the computation procedure:

(a) A large-scale plot of the airfoil (fig. 14 (a))

(b) A plot of s/c versus x for both upper and lower surfaces (fig. 14 (b))

(c) A plot of k for various x positions (fig. 14 (c))

(d) Chordwise distribution of incompressible-flow air velocities over the airfoil surface (fig. 14 (d)).

Step 2.—Construct an air hodograph (fig. 14 (e)) from the information in figures 14 (c) and 14 (d).

Step 3.—Construct a drop hodograph (fig. 14 (f)) using as aids the air hodograph of step (2), fig. 6, and equation (5).

Step 4.—Estimate values of drop acceleration at the airfoil surface (fig. 14 (g)) with the aid of equations (8) and (9), and the known condition of zero drop acceleration at the extreme position of tangential drop inpingement.

Step 5.—Compute values of the scale modulus, corresponding to selected values of s/c, by using equation (4). Values of R/R_V, a_d, and $C_dR/24$ employed in equation (4) are obtained from figures 14 (f), (g), and (h), respectively.

Step 6.—Plot curves of s/c versus ψ for isopleths of R_V (fig. 14 (i)) using the calculated points from step (5). Values of ψ for $s/c=0$ are obtained for this plot by using equation (13) in conjunction with figure 10.

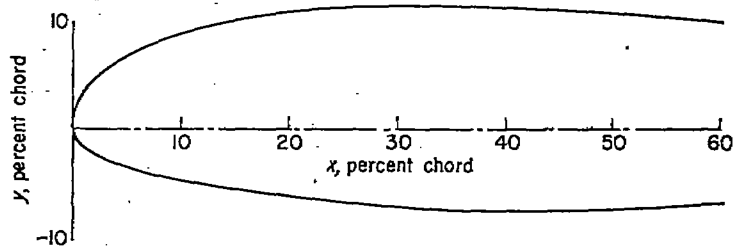

(a) Airfoil contour.

FIGURE 14.—Graphical relationships used in evaluating farthest position of impingement for an NACA 23015 airfoil; $c_l=0.5$; $\alpha=3.6°$.

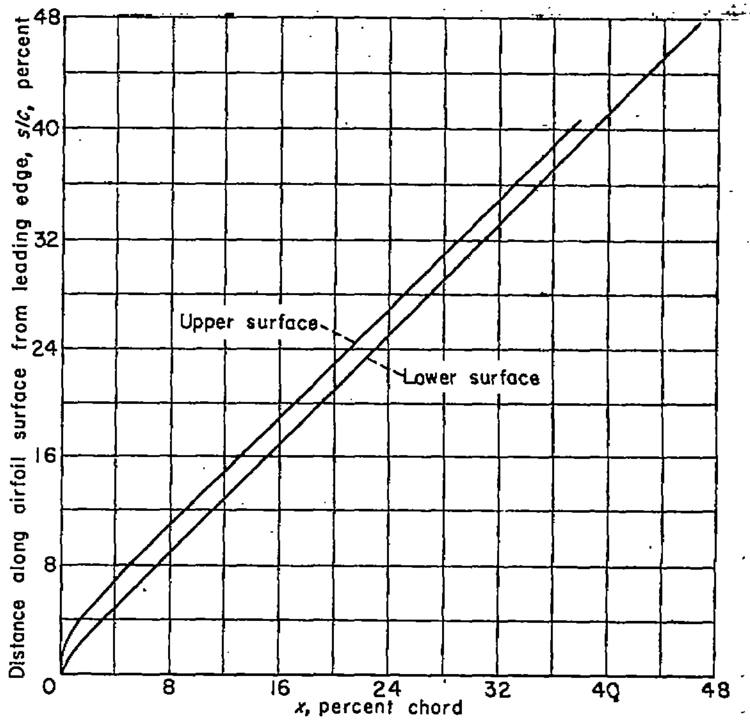

(b) Variation of s/c with chordwise position.

FIGURE 14.—Continued.

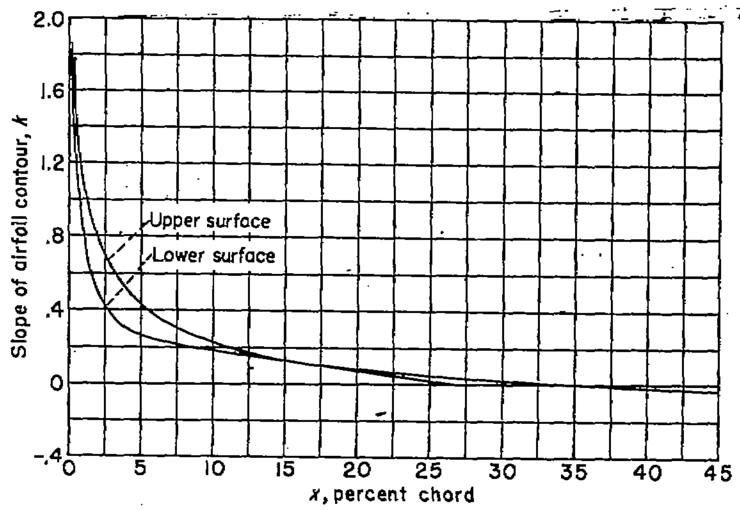

(c) Slope of airfoil contour as a function of chordwise position.

FIGURE 14.—Continued.

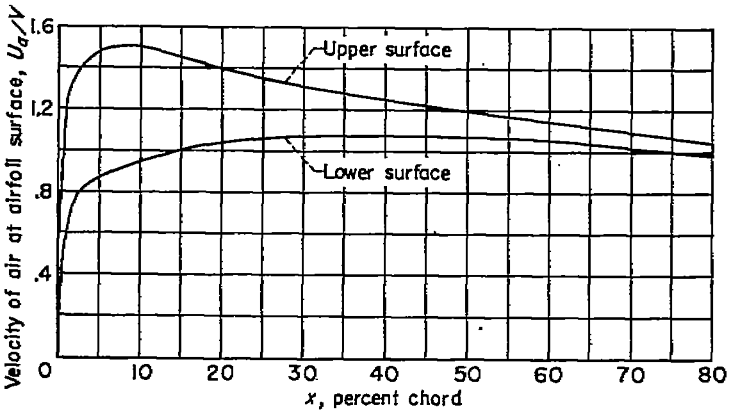

(d) Chordwise velocity distribution.

FIGURE 14.—Continued.

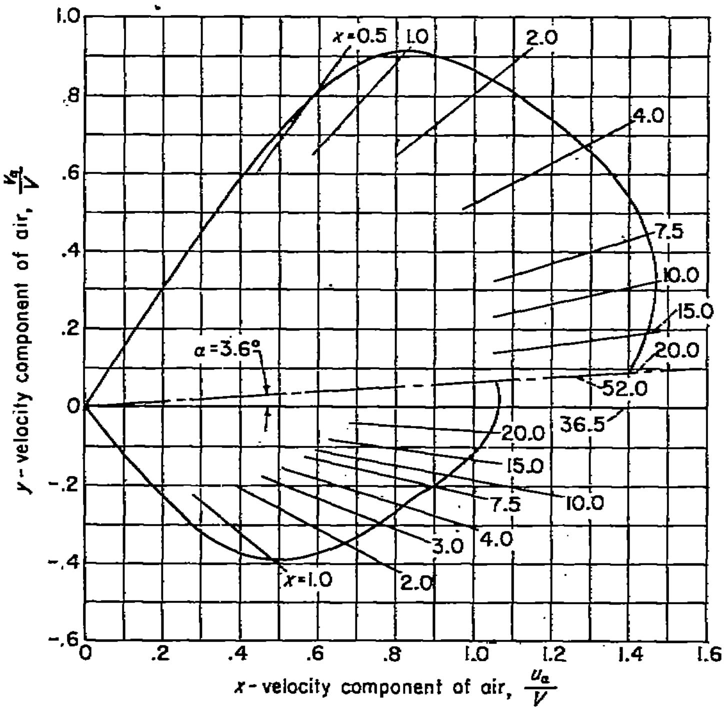

(e) Hodograph for air.

FIGURE 14.—Continued.

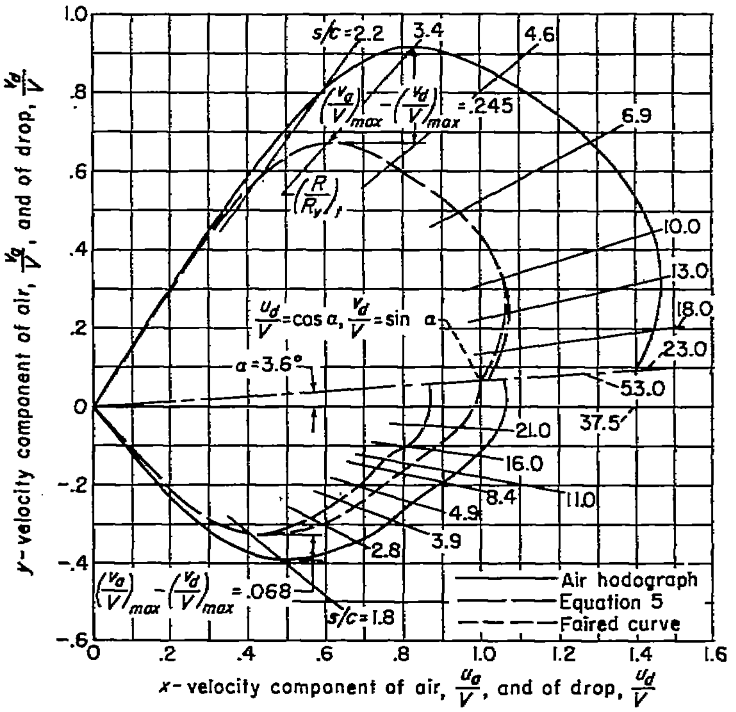

(f) Drop hodograph constructed from air hodograph.

FIGURE 14.—Continued.

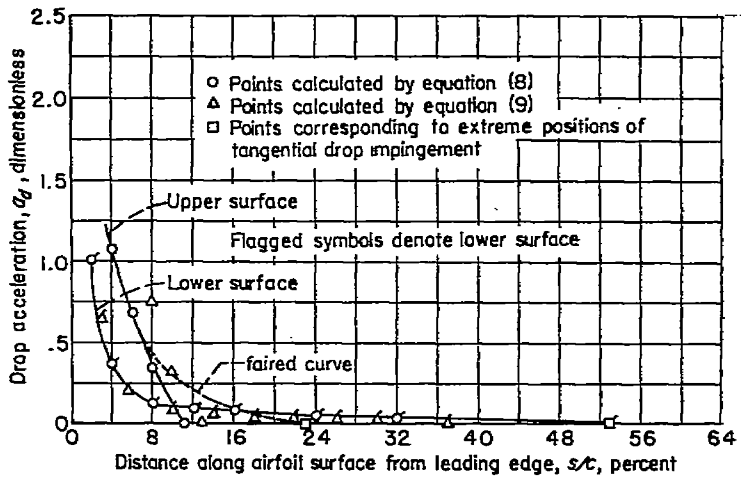

(g) Distribution of drop acceleration values over airfoil surface.

FIGURE 14.—Continued.

RATE OF IMPINGEMENT

The procedure for determining total rate of impingement, as has been explained in reference 1, consists of summing the rate of water-drop impingement for each of the drop sizes in an assumed drop-size distribution. A summation is possible for each size of drop by use of the equation:

$$M_t = 3600\, EVmy_{max}$$

The values of V, m, and y_{max} are obtainable directly from a knowledge of the nature of the icing conditions and the airfoil shape. The procedure for calculating efficiency of impingement consists essentially of evaluating equation (15). The following steps, with the aid of figure 15, are intended to explain how the evaluation of equation (15) is performed:

Step 1.—Establish the following relationships for use during the computation procedure: s/c as a function of y/c for both upper and lower surfaces (fig. 15 (a)), and y_t as a function of ψ for the desired values of R_V (fig. 15 (b)). Figure 15 (b) is obtained from figure 14 (i) by employing the conversion relation between s/c and y/c (fig. 15 (a)). In figure 15 (b), use is made of figure 11 to establish the value of ψ which corresponds to the value of $(\Delta y_o/\Delta y)_t=0.8$.

Step 2.—Construct $(\Delta y_o/\Delta y)_t$ as a linear function of ψ on semilogarithmic coordinate paper for the desired values of R_V (fig. 15 (c)). Two points are required to establish the function for each value of R_V. One point is obtained from equation (13) already discussed in step (6) under area of impingement; the other point is obtained through the aid of figure 15 (b).

Step 3.—Calculate values of impingement efficiency using equation (15). Values of $(\Delta y_o/\Delta y)_t$ and Δy_t used are obtained from figures 15 (b) and 15 (c), respectively. Results of calculations for the NACA 23015 airfoil are shown in figure 15 (d).

DISTRIBUTION OF IMPINGEMENT

Distribution of impingement is considered defined, as explained in reference 1, when values of the concentration

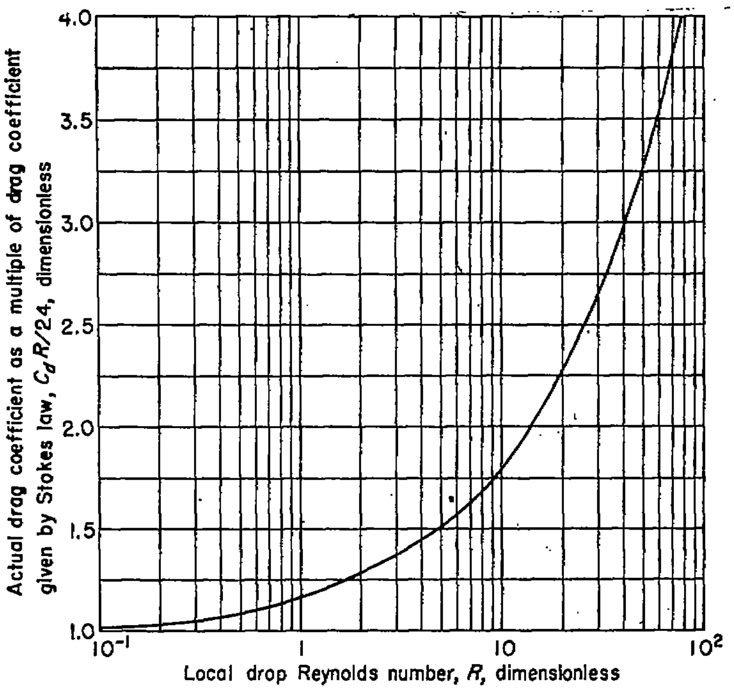

(h) $\frac{C_dR}{24}$ as a function of R.

FIGURE 14.—Continued.

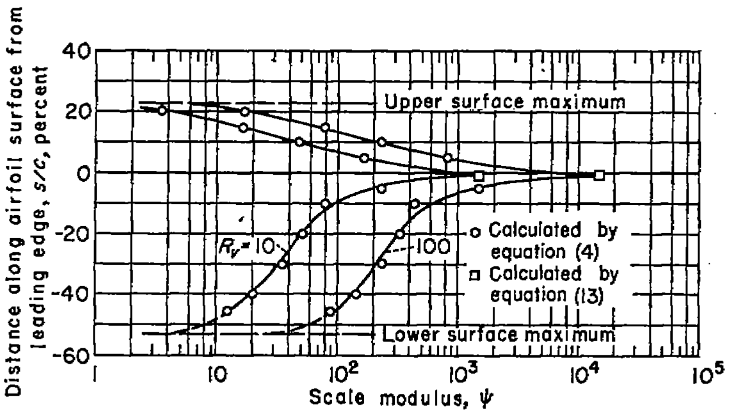

(i) Farthest position of impingement as a function of scale modulus.

FIGURE 14.—Concluded.

factor C are determined over the region of drop impingement. A summary of the procedure to establish these values is as follows:

Step 1.—Determine a limit distribution curve of C versus s/c by equation (18). To evaluate equation (18), a plot of y_o' versus s/c is required (fig. 16 (a)) for straight-line trajectories. Figure 16 (a) can be established with the aid of a graphical construction of straight-line trajectories impinging on the airfoil being considered (fig. 16 (b)). A limit distribution is shown in figure 16 (c) for the NACA 23015 airfoil.

Step 2.—Construct a triangular distribution of impingement of C versus s/c. To establish this distribution, three values of C are located on the plot. One of these values is given by equation (19) and is located on a line connecting the points $C=1.0$, $s/c=0$, and $C=0$, and s/c for the stagnation point. The other two points are located at a value of $C=0$ at values of s/c for farthest positions of impingement. Figure 16 (c) shows a triangular distribution for the NACA 23015 airfoil.

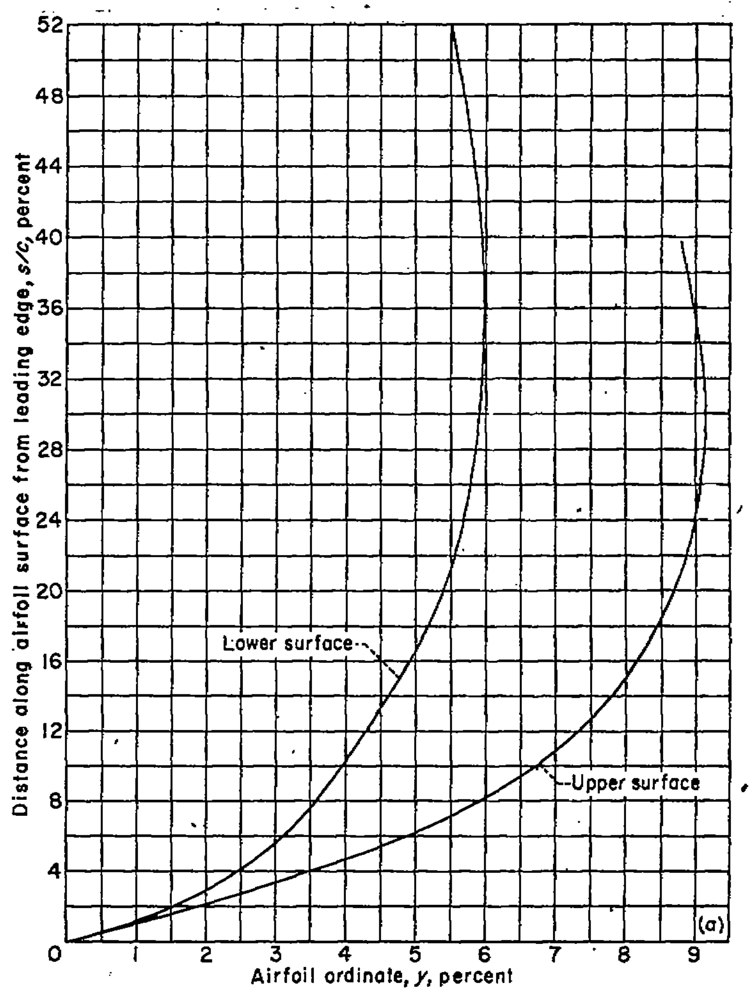

(a) Variation of s/c with airfoil ordinates.

FIGURE 15.—Graphical relationships used in evaluating impingement efficiency for an NACA 23015 airfoil; $c_l=0.5$; $\alpha=3.6°$.

Step 3.—Modify the triangular distribution established in step 2 to conform with the general shape of the limit distribution found in step 1. In performing the modification, the area contained within the new distribution curve is made equal to that contained within the triangular distribution. This condition usually results in a larger value of C_{max}. A modified distribution curve is shown in figure 16 (c) for a particular combination of ψ and R_V.

EVALUATION OF THE PROCEDURE DESCRIBED IN THIS REPORT

The degree to which the final values of farthest position and efficiency of drop impingement, as estimated herein, depend upon the accuracy of determination of the intermediate quantities $(R/R_V)_i$, a_d, and G was investigated by determining the effect of arbitrarily altering these three quantities a given percentage. By this means, the effect on farthest position and efficiency of impingement can be appraised for the selected changes in the three variables; also, some measure is obtained of the error introduced by the approximations used in the calculation procedure.

When computations were made for the 15-percent-thick symmetrical Joukowski airfoil at $\alpha=4°$, and the values of $(R/R_V)_i$, a_d, and G were altered by ± 10 percent in all possible combinations, it was found that in no case was changing G

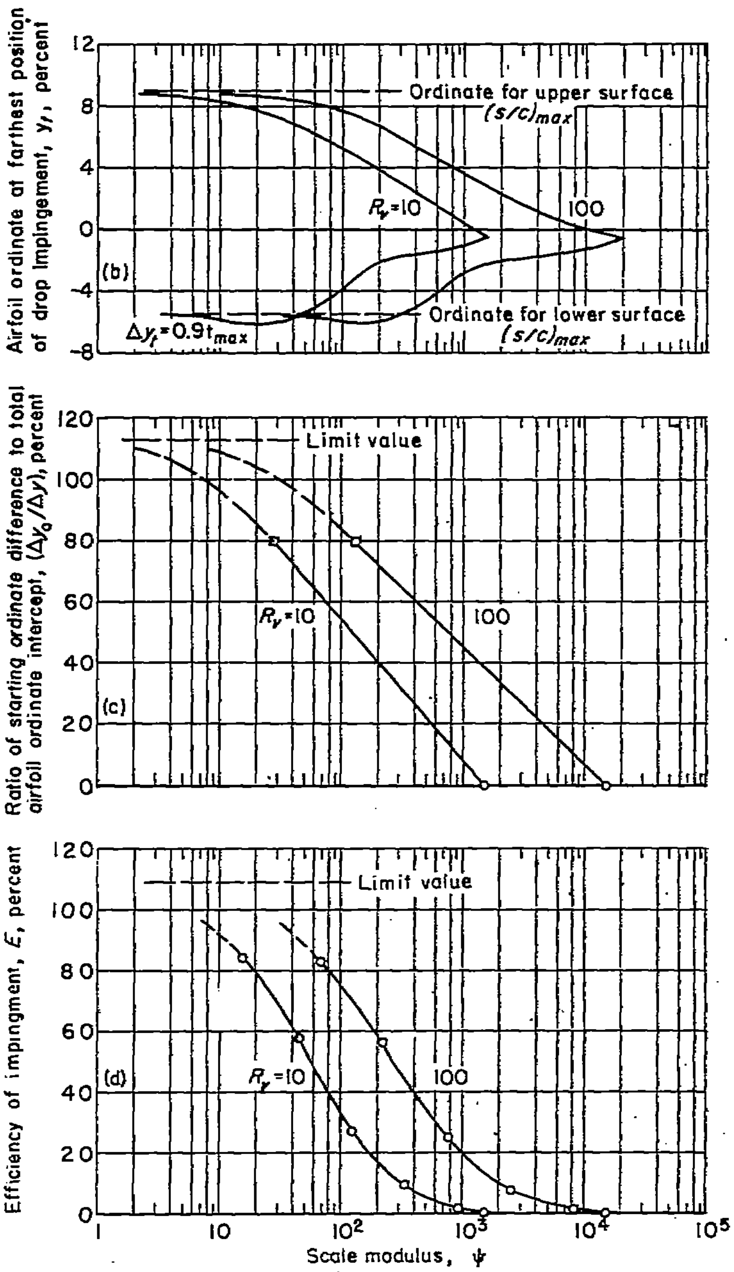

(b) Airfoil ordinate at farthest position of impingement.
(c) Ordinate-ratio isopleths.
(d) Efficiency of impingement.

FIGURE 15.—Concluded.

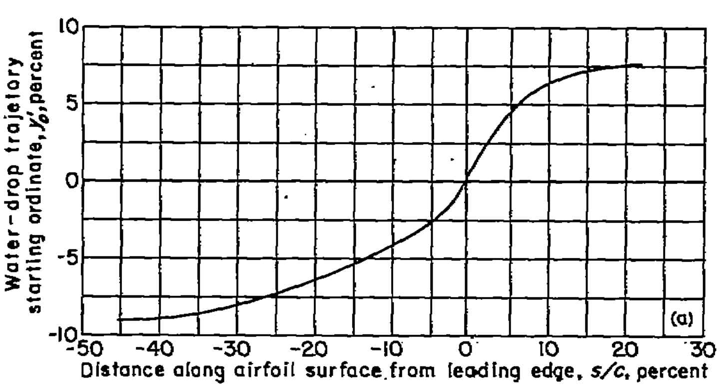

(a) Straight-line trajectory starting ordinates as a function of s/c.

FIGURE 16.—Graphical relationships used in evaluating distribution of impingement for an NACA 23015 airfoil; c_l=0.5; α=3.6°.

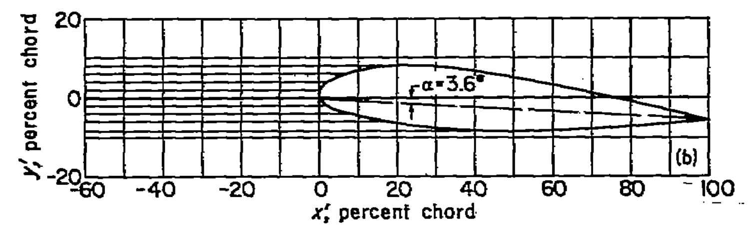

(b) Straight-line trajectories impinging an airfoil.

FIGURE 16.—Continued.

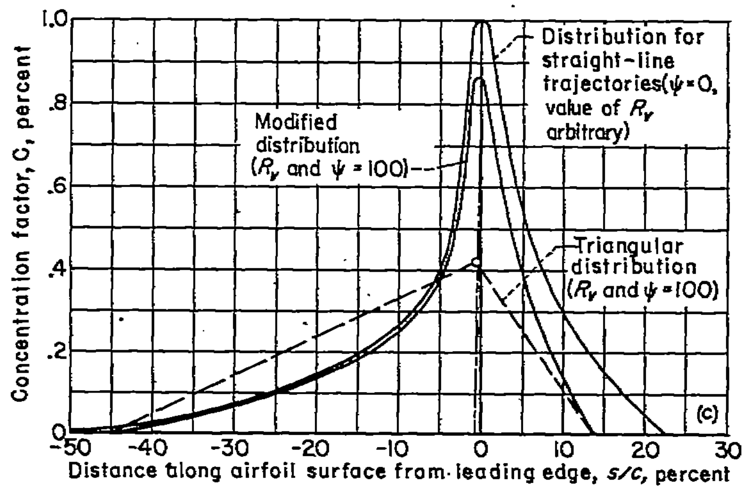

(c) Distribution of impingement.

FIGURE 16.—Concluded.

significant for farthest position of impingement. The combination of positive and negative changes providing the largest change in ψ resulted in a change in s/c of about 2-percent chord over most of the range in values of ψ. The approximations contributed an additional change of only about ½-percent chord.

For efficiency of impingement, the effect of a change in the term G alone was to make a change in efficiency of about 0.5 percent; the combination of positive and negative changes in $(R/R_V)_t$ and a_s providing maximum change in ψ made a change in efficiency of about 3 percent over most of the range in ψ values. As compared with these changes, the approximations led to efficiency of impingement values which differed from the differential analyzer values by about −15 percent.

While the foregoing values will not necessarily be representative for all other airfoils, they probably indicate the order of magnitude of error in area and efficiency of impingement to be expected when the error in the terms $(R/R_V)_t$, a_s, and G can be kept within ±10 percent. Whether this sort of accuracy always can be realized by using the procedures suggested in this report can be ascertained only as more water-drop-trajectory data become available.

CONCLUDING REMARKS

Results of water-drop-trajectory data obtained from a differential analyzer have indicated trends which were used as a basis for devising a procedure for calculating area, rate, and distribution of water-drop impingement on airfoil sections of arbitrary profile. These trends are more firmly established for airfoils resembling the Joukowski airfoils investigated than for low-drag airfoils, since the basic data were obtained for four Joukowski airfoil cases and only one low-drag section. Further water-drop-trajectory data are needed, particularly for thin airfoils (order of 5 percent thick) at high speeds, and airfoils at high angle of attack (in the neighborhood of 12°). Whether these new data would make it necessary to revise the concepts presented herein, replace, or substantiate them remains to be seen. Until such data are available, however, the method derived from these trajectory data should permit more complete and accurate calculations of the area, rate, and distribution of water-drop impingement on an arbitrary airfoil than other semiempirical methods.

AMES AERONAUTICAL LABORATORY
NATIONAL ADVISORY COMMITTEE FOR AERONAUTICS
MOFFETT FIELD, CALIF., *May 8, 1951*

REFERENCES

1. Neel, Carr B., Bergrun, Norman R., Jukoff, David, and Schlaff, Bernard A.: The Calculation of the Heat Required for Wing Thermal Ice Prevention in Specified Icing Conditions. NACA TN 1472, 1947.
2. Patterson, D. M.: A Simplified Procedure for the Determination of Heat Requirements for Ice Protection of Fixed Areas of Aircraft. Central Air Documents Office, Technical Data Digest, vol. 14, no. 4, February 15, 1949, pp. 15–23.
3. Bergrun, Norman R.: A Method for Numerically Calculating the Area and Distribution of Water Impingement on the Leading Edge of an Airfoil in a Cloud. NACA TN 1397, 1947.
4. Neel, Carr B., Jr.: Calculation of Heat Required for Wing Thermal Ice Prevention in Specified Icing Conditions. S. A. E. Quarterly Transactions, vol. 2, no. 3, July 1948, pp. 369–378.
5. Bergrun, Norman R.: An Empirical Method Permitting Rapid Determination of the Area, Rate, and Distribution of Water-Drop Impingement on an Airfoil of Arbitrary Section at Subsonic Speeds. NACA TN 2476, 1951.
6. Guibert, A. G., Janssen, E., and Robbins, W. M.: Determination of Rate, Area, and Distribution of Impingement of Waterdrops on Various Airfoils from Trajectories Obtained on the Differential Analyzer. NACA RM 9A05, 1949.
7. Langmuir, Irving, and Blodgett, Katherine B.: A Mathematical Investigation of Water Droplet Trajectories. General Electric Co. Rep., 1945.
8. Glauert, Muriel: A Method of Constructing the Paths of Raindrops of Different Diameters Moving in the Neighborhood of (1) a Circular Cylinder, (2) an Aerofoil, Placed in a Uniform Stream of Air; and a Determination of the Rate of Deposit of the Drops on the Surface and the Percentage of Drops Caught. R. & M. No. 2025, British A. R. C., 1940.
9. Tribus, Myron: Modern Icing Technology. Lecture Notes. Project M992-E. Univ. of Mich. Eng. Research Institute, Jan. 1952.

TABLE I.—RESULTS FROM DIFFERENTIAL ANALYZER STUDIES OF WATER-DROP IMPINGEMENT ON A 15-PERCENT-THICK SYMMETRICAL JOUKOWSKI AIRFOIL

[$c_l=0$; $\alpha=0°$]

ψ	R_V	y_o	Surface	s/c	u_d/V	v_d/V
2	128	0.074	Upper [1]	0.265	1.0	0
2	128	−.074	Lower [1]	−.265	1.0	0
8	512	.074	Upper [1]	.273	.997	.004
8	512	−.074	Lower [1]	−.273	.997	−.004
32	2048	.072	Upper [1]	.262	.997	.013
32	2048	−.072	Lower [1]	−.262	.997	−.013
4	32	.073	Upper [1]	.273	1.0	.012
4	32	−.073	Lower [1]	−.273	1.0	−.012
16	128	.070	Upper [1]	.244	1.005	.023
16	128	.045	do	.068	.99	.013
16	128	.020	do	.021	.962	.009
16	128	−.020	Lower	−.021	.962	−.009
16	128	−.045	do	−.068	.99	−.013
16	128	−.070	Lower [1]	−.244	1.005	−.023
64	512	.0655	Upper [1]	.225	1.004	.043
64	512	−.0655	Lower [1]	−.225	1.004	−.043
256	2048	.058	Upper [1]	.188	1.007	.092
256	2048	.040	Upper	.058	.949	.069
256	2048	.020	do	.023	.931	.029
256	2048	−.020	Lower	−.023	.931	−.029
256	2048	−.040	do	−.058	.949	−.069
256	2048	−.058	Lower [1]	−.188	1.007	−.092
8	8	.059	Upper [1]	.197	.994	.078
8	8	−.059	Lower [1]	−.197	.994	−.078
32	32	.056	Upper [1]	.185	.992	.089
32	32	−.056	Lower [1]	−.185	.992	−.089
128	128	.0485	Upper [1]	.150	.989	.149
128	128	−.0485	Lower [1]	−.150	.989	−.149
512	512	.038	Upper [1]	.108	.941	.225
512	512	−.038	Lower [1]	−.108	.941	−.225
2048	2048	.025	Upper [1]	.072	.856	.349
2048	2048	−.025	Lower [1]	−.072	.856	−.349
64	8	.0255	Upper [1]	.078	.870	.321
64	8	.018	do	.031	.693	.192
64	8	.008	do	.010	.698	.061
64	8	−.008	Lower	−.010	.696	−.061
64	8	−.018	do	−.031	.693	−.192
64	8	−.0255	Lower [1]	−.078	.870	−.321
256	32	.021	Upper [1]	.073	.828	.359
256	32	−.021	Lower [1]	−.073	.828	−.359
1024	128	.015	Upper [1]	.052	.741	.451
1024	128	.010	Upper	.020	.572	.198
1024	128	.005	do	.009	.563	.109
1024	128	−.005	Lower	−.009	.563	−.109
1024	128	−.010	do	−.020	.572	−.198
1024	128	−.015	do	−.052	.741	−.451
4096	512	.0110	Upper [1]	.038	.584	.452
4096	512	−.0110	Lower [1]	−.038	.584	−.452
16384	2048	.004	Upper [1]	.022	.329	.469
16384	2048	−.004	Lower [1]	−.022	.329	−.469
512	8	.0035	Upper [1]	.023	.355	.514
512	8	−.0035	Lower [1]	−.023	.355	−.514
8192	128	.0020	Upper [1]	.015	.251	.401
8192	128	−.0020	Lower [1]	−.015	.251	−.401
32768	512	.0005	Upper [1]	.016	.187	.459
32768	512	−.0005	Lower [1]	−.016	.187	−.459

[1] Denotes tangential trajectories.

TABLE II.—RESULTS FROM DIFFERENTIAL ANALYZER STUDIES OF WATER-DROP IMPINGEMENT ON A 15-PERCENT-THICK SYMMETRICAL JOUKOWSKI AIRFOIL

[$c_l=0.22$; $\alpha=2°$]

ψ	R_V	y_o	Surface	s/c	u_d/V	v_d/V
4	256	−0.0046	Upper [1]	0.236	1.001	0.041
4	256	−.1548	Lower [1]	−.316	.998	.035
16	1024	−.0055	Upper [1]	.228	1.003	.044
16	1024	−.1539	Lower [1]	−.310	.998	.030
2	16	−.0061	Upper [1]	.226	1.009	.053
2	16	−.1533	Lower [1]	−.311	.997	.027
8	64	−.0095	Upper [1]	.212	1.011	.062
8	64	−.0381	do	.045	.963	.054
8	64	−.0667	do	.005	.964	.044
8	64	−.0956	Lower	−.026	.974	.039
8	64	−.1243	do	−.062	.972	.033
8	64	−.1652	Lower [1]	−.308	.997	.022
32	256	−.0140	Upper [1]	.196	1.015	.063
32	256	−.0410	do	.041	.960	.066
32	256	−.0683	do	.003	.969	.052
32	256	−.0958	Lower	−.026	.970	.038
32	256	−.1232	do	−.078	.975	.024
32	256	−.1506	Lower [1]	−.295	.995	.013
128	1024	−.0214	Upper [1]	.168	1.021	.126
128	1024	−.0404	do	.034	.958	.100
128	1024	−.0721	do	.002	.941	.063
128	1024	−.0977	Lower	−.027	.939	.032
128	1024	−.1231	do	−.079	.955	.004
128	1024	−.1458	do	−.265	.992	−.006
16	16	−.0435	Upper [1]	.149	1.010	.160
16	16	−.1536	Lower [1]	−.245	.964	−.023
64	64	−.0433	Upper [1]	.128	1.012	.202
64	64	−.0705	do	.027	.906	.140
64	64	−.0902	Lower	−.001	.881	.083
64	64	−.1130	do	−.027	.881	.033
64	64	−.1345	do	−.071	.921	−.013
64	64	−.1558	Lower [1]	−.225	.963	−.052
256	256	−.0587	Upper [1]	.100	.999	.283
256	256	−.0763	do	.022	.852	.189
256	256	−.0640	Lower	−.002	.827	.103
256	256	−.1118	do	−.023	.815	.015
256	256	−.1298	do	−.058	.863	−.050
256	256	−.1475	do. [1]	−.177	.963	−.105
1024	1024	−.0743	Upper [1]	.063	.914	.424
1024	1024	−.1360	Lower [1]	−.118	.902	−.195
128	16	−.0955	Upper [1]	.055	.881	.472
128	16	−.1065	do	.009	.640	.235
128	16	−.1160	Lower	−.004	.637	.113
128	16	−.1250	do	−.017	.642	−.006
128	16	−.1335	do	−.036	.685	−.109
128	16	−.1430	Lower [1]	−.098	.854	−.246
512	64	−.1005	Upper [1]	.038	.767	.528
512	64	−.1080	do	.009	.560	.270
512	64	−.1155	Lower	−.004	.542	.132
512	64	−.1230	do	−.016	.535	−.011
512	64	−.1310	do	−.03	.611	−.140
512	64	−.1382	do. [1]	−.079	.813	−.300
2048	256	−.1085	Upper [1]	.028	.582	.611
2048	265	−.1130	do	.004	.394	.265
2048	256	−.1182	Lower	−.005	.379	.118
2048	256	−.1228	do	−.014	.377	−.050
2048	256	−.1275	do	−.029	.500	−.235
2048	256	−.1325	do. [1]	−.055	.688	−.356
8192	1024	−.1165	Upper [1]	.015	.210	.514
8192	1024	−.1190		0	.270	.230
8192	1024	−.1218	Lower	−.004	.260	.065
8192	1024	−.1250	do	−.012	.273	−.110
8192	1024	−.1275	do. [1]	−.031	.520	−.390
1024	16	−.1232	Upper [1]	.008	.156	.610
1024	16	−.1262	Lower [1]	−.015	.100	−.243
4096	64	−.1243	Upper [1]	.003	.090	.434
4096	64	−.1278	Lower [1]	−.015	.246	−.235
16384	256	−.1254	Upper [1]	.002	.103	.506
16384	256	−.1275	Lower [1]	−.014	.175	.295

[1] Denotes tangential trajectories.

TABLE III.—RESULTS FROM DIFFERENTIAL ANALYZER STUDIES OF WATER-DROP IMPINGEMENT ON A 15-PERCENT-THICK SYMMETRICAL JOUKOWSKI AIRFOIL

[$c_l=0.44$; $\alpha=4°$]

ψ	R_V	y_o	Surface	s/c	u_d/V	v_d/V
4	256	−0.1662	Upper [1]	0.204	0.9996	0.0785
4	256	−.3215	Lower [1]	−.408	.9946	.0705
16	1024	−.1692	Upper [1]	.194	1.0066	.1005
16	1024	−.3223	Lower [1]	−.400	.9976	.0705
2	16	−.1818	Upper [1]	.192	1.0034	.0962
2	16	−.3330	Lower [1]	−.409	.9891	.0668
8	64	−.1837	Upper [1]	.170	1.0055	.1082
8	64	−.3073	Lower	−.135	.9602	.0728
8	64	−.2624	do	−.064	.9782	.0789
8	64	−.2577	do	−.024	.9663	.1120
8	64	−.2330	Upper	.004	.9793	.0940
8	64	−.2083	do	.037	.9854	.1011
8	64	−.3320	Lower [1]	−.400	.9930	.0638
32	256	−.1881	Upper [1]	.148	1.0174	.1381
32	256	−.2121	do	.034	.9764	.1221
32	256	−.2358	do	.002	.9653	.1050
32	256	−.2504	Lower	−.024	------	------
32	256	−.2832	do	−.062	------	------
32	256	−.3068	do	−.124	.9652	.0628
32	256	−.3316	do	−.379	.9831	.0618
128	1024	−.1994	Upper [1]	.127	1.0294	.2031
128	1024	−.2074	do	.062	.9804	.0931
128	1024	−.2205	do	.028	.9514	.1670
128	1024	−.2386	do	.004	.9304	.1410
128	1024	−.2748	Lower	−.041	.9273	.0869
128	1024	−.3077	do	−.125	.9433	.0519
128	1024	−.3316	do	−.350	1.0200	.0468
16	16	−.2403	Upper [1]	.121	1.0116	.2241
16	16	−.3865	Lower [1]	−.336	.9628	.0415
64	64	−.2472	Upper [1]	.100	1.0133	.2681
64	64	−.3422	Lower	−.113	.8940	.0448
64	64	−.3231	do	−.060	.8712	.0731
64	64	−.3043	do	−.028	.8694	.1147
64	64	−.2853	do	−.004	.8638	.1675
64	64	−.2665	Upper	.018	.8990	.2148
64	64	−.3606	Lower [1]	−.286	.9578	.0135
256	256	−.2622	Upper [1]	.068	1.0121	.4068
256	256	−.2775	do	.012	.8138	.2746
256	256	−.2925	Lower	−.008	.7827	.1843
256	256	−.3078	do	−.028	.7864	.1092
256	256	−.3353	do	−.084	.8281	.0149
256	256	−.3444	do	−.125	.8660	.0142
256	256	−.3537	do. [1]	−.247	.9558	−.0313
1024	1024	−.2762	Upper [1]	.043	.8758	.5817
1024	1024	−.3440	Lower [1]	−.155	.8780	−.1212
128	16	−.3126	Upper [1]	.042	.8255	.5550
128	16	−.3598	Lower	−.067	.7143	.0364
128	16	−.3500	do	−.040	.6586	.0228
128	16	−.3406	do	−.022	.6048	.1031
128	16	−.3313	do	−.006	.615	.2444
128	16	−.3220	Upper	−.006	.6562	.3437
128	16	−.3688	Lower [1]	−.145	.8632	−.1358
512	64	−.3216	Upper [1]	.026	.6392	.7017
512	64	−.3303	Lower	−.004	.5021	.3024
512	64	−.3363	do	−.015	.4678	.1513
512	64	−.3441	do	−.027	.5197	.0390
512	64	−.3500	do	−.042	.5566	−.0782
512	64	−.3558	do	−.062	.6465	−.1363
512	64	−.3605	do. [1]	−.112	.8133	−.2045
2048	256	−.3293	Upper [1]	.015	.4240	.7513
2048	256	−.3324	do	.002	.3300	.4553
2048	256	−.3373	Lower	−.008	.2858	.2442
2048	256	−.3432	do	−.022	.3548	.0060
2048	256	−.3471	do	−.032	.4137	−.1191
2048	256	−.3501	do	−.045	.4956	−.1923
2048	256	−.3529	do. [1]	−.072	.6575	−.2912
8192	1024	−.3382	Upper [1]	.004	.0918	.7521
8192	1024	−.3405	Lower	−.005	.1918	.4371
8192	1024	−.3441	do	−.012	.1787	.1520
8192	1024	−.3458	do	−.020	.2787	.0669
8192	1024	−.3474	do	−.031	.2867	−.2011
8192	1024	−.3480	do. [1]	−.041	.4156	−.2832
1024	16	−.3495	Upper [1]	.004	.1147	.6545
1024	16	−.3544	Lower [1]	−.035	.3498	−.2806
4096	64	−.3495	Upper [1]	.002	.1047	.6945
4096	64	−.3530	Lower [1]	−.026	.2146	−.2157
16384	256	−.3504	Upper [1]	.002	.1597	.5494
16384	256	−.3536	Lower [1]	−.025	.2746	−.2256

[1] Denotes tangential trajectories.

TABLE IV.—RESULTS FROM DIFFERENTIAL ANALYZER STUDIES OF WATER-DROP IMPINGEMENT ON A 15-PERCENT-THICK CAMBERED JOUKOWSKI AIRFOIL

[a=1.0 MEAN LINE; c_l=0.44; α=0°]

ψ	R_V	y_o	Surface	s/c	u_d/V	v_d/V
4	256	0.0935	Upper [1]	0.317	1.003	0.007
4	256	−.0565	Lower [1]	−.216	.996	−.002
16	1024	.0915	Upper [1]	.310	1.008	.013
16	1024	−.0565	Lower [1]	−.213	.999	−.006
2	16	.0855	Upper [1]	.305	1.009	.022
2	16	−.0600	Lower [1]	−.215	.994	−.001
8	64	.0818	Upper [1]	.294	1.012	.031
8	64	.0536	do	.096	.992	.022
8	64	.0253	do	.038	.988	.020
8	64	−.0038	do	.002	.985	.011
8	64	−.0318	Lower	−.033	.984	.003
8	64	−.0610	do. [1]	−.212	.999	−.008
32	256	.0775	Upper [1]	.275	1.022	.050
32	256	.0503	do	.092	.989	.042
32	256	.0225	do	.034	.976	.030
32	256	−.0045	do	.001	.972	.017
32	256	−.0325	Lower	−.033	.973	.002
32	256	−.0600	do. [1]	−.199	.990	−.016
128	1024	.0660	Upper [1]	.243	1.033	.090
128	1024	.0420	do	.077	.976	.075
128	1024	.0160	do	.030	.954	.054
128	1024	−.0085		0	.943	.024
128	1024	−.0335	Lower	−.032	.946	−.006
128	1024	−.0585	do. [1]	−.183	.984	−.036
16	16	.0377	Upper [1]	.211	1.028	.128
16	16	−.0770	Lower [1]	−.180	.978	−.042
64	64	.0312	Upper [1]	.192	1.038	.168
64	64	.0100	do	.061	.936	.131
64	64	−.0110	do	.022	.898	.095
64	64	−.0315	Lower	−.003	.884	.048
64	64	−.0525	do	−.031	.891	−.007
64	64	−.0731	do. [1]	−.157	.971	−.073
256	256	.0180	Upper [1]	.158	1.038	.238
256	256	.0010	do	.050	.893	.188
256	256	−.0165	do	.018	.839	.127
256	256	−.0340	Lower	−.004	.820	.054
256	256	−.0510	do	−.028	.838	−.017
256	256	−.0680	do	−.120	.940	−.129
1024	1024	0	Upper [1]	.109	1.000	.357
1024	1024	−.0620	Lower [1]	−.085	.883	−.220
128	16	−.028	Upper [1]	.092	.958	.405
128	16	−.0382	do	.032	.727	.288
128	16	−.0480	do	.012	.638	.189
128	16	−.0575	Lower	−.004	.649	.060
128	16	−.0670	do	−.019	.644	−.046
128	16	−.0772	do. [1]	−.068	.838	−.264
512	64	−.0347	Upper [1]	.072	.911	.487
512	64	−.0425	do	.025	.634	.350
512	64	−.150	do	.010	.535	.208
512	64	−.0582	Lower	−.005	.485	.031
512	64	−.066	do	−.018	.544	−.124
512	64	−.0725	do. [1]	−.053	.754	−.319
2048	256	−.0440	Upper [1]	.046	.686	.576
2048	256	−.050	do	.015	.448	.360
2048	256	−.0548	do	.005	.381	.192
2048	256	−.0594	Lower	.004	.368	.048
2048	256	−.0638	do	−.013	.407	−.103
2048	256	−.0685	Lower [1]	−.038	.604	−.384
8192	1024	−.0548	Upper [1]	.025	.471	.650
8192	1024	−.0569	do	.007	.258	.308
8192	1024	−.0590	Lower	−.001	.178	.082
8192	1024	−.0610	do	−.008	.184	−.079
8192	1024	−.0630	do	−.012	.211	−.168
8192	1024	−.0650	do. [1]	−.025	.464	−.428
1024	16	−.0604	Upper [1]	.022	.346	.561
1024	16	−.0700	Lower [1]	−.018	.317	−.368
4096	64	−.0650	Upper [1]	.015	.285	.527
4096	64	−.0675	Lower [1]	−.012	.143	−.253
16384	256	−.0655	Upper [1]	.006	.113	.391
16384	256	−.0670	Lower [1]	−.008	.046	−.118

[1] Denotes tangential trajectories.

TABLE V.—RESULTS FROM DIFFERENTIAL ANALYZER STUDIES OF WATER-DROP IMPINGEMENT ON AN NACA 65_1–015 AIRFOIL

[c_l=0.44; α=4°]

ψ	R_V	y_o	Surface	s/c	u_d/V	v_d/V
4	256	−0.1281	Upper [1]	0.281	1.0023	0.0814
4	256	−.2817	Lower [1]	−.523	.9973	.0704
16	1024	−.1298	Upper [1]	.267	1.0073	.0804
16	1024	−.2818	Lower [1]	−.514	.9973	.0704
2	16	−.1395	Upper [1]	.259	1.0047	.0945
2	16	−.1646	do	.031	.9881	.0875
2	16	−.2026	Lower	−.022	.9847	.0825
2	16	−.2246	do	−.074	.9807	.0793
2	16	−.2467	do	−.160	.9857	.0753
2	16	−.2687	do	−.256	.9847	.0742
2	16	−.2909	do. [1]	−.514	.9927	.0711
8	64	−.1424	Upper [1]	.240	1.0107	.1065
8	64	−.1719	do	.016	.9847	.0935
8	64	−.2163	Lower	−.050	.9757	.0824
8	64	−.2409	do	−.125	.9807	.0743
8	64	−.2655	do	−.236	.9797	.0712
8	64	−.2899	do. [1]	−.512	.9907	.0641
32	256	−.1493	Upper [1]	.209	1.0187	.1320
32	256	−.1702	do	.023	.9761	.1156
32	256	−.2193	Lower	−.052	.9617	.0874
32	256	−.2437	do	−.131	.9647	.0743
32	256	−.2685	do	−.249	.9717	.0032
32	256	−.2894	do. [1]	−.506	1.0057	.0631
128	1024	−.1603	Upper [1]	.160	1.0207	.1805
128	1024	−.1826	do	.008	.9517	.1375
128	1024	−.2282	Lower	−.068	.9427	.0853
128	1024	−.2505	do	−.145	.9407	.0042
128	1024	−.2726	do	−.267	.9557	.0462
128	1024	−.2878	do. [1]	−.485	.9837	.0382
16	16	−.1951	Upper [1]	.128	1.0015	.2008
16	16	−.3202	Lower [1]	−.481	.9775	.0383
64	64	−.2030	Upper [1]	.092	.9956	.2597
64	64	−.2136	do	.012	.9156	.2055
64	64	−.2535	Lower	−.048	.8795	.1092
64	64	−.2787	do	−.127	.8975	.0609
64	64	−.3013	do	−.247	.9255	.0227
64	64	−.3111	do. [1]	−.417	.9756	.0074
256	256	−.2143	Upper [1]	.047	.9416	.3416
256	256	−.2343	Lower	−.007	.8256	.1904
256	256	−.2543	do	−.040	.8080	.1102
256	256	−.2717	do	−.093	.8310	.0410
256	256	−.2892	do	−.184	------	------
256	256	−.2983	do. [1]	−.355	.9085	−.0443
1024	1024	−.2267	Upper [1]	.026	.8575	.4614
1024	1024	−.2313	do	.010	.7726	.3935
1024	1024	−.2492	Lower	−.015	.6715	.1972
1024	1024	−.2692	do	−.060	.6295	.0300
1024	1024	−.2782	do	−.104	.7875	−.0251
1024	1024	−.2853	do	−.166	.7495	−.0692
1024	1024	−.2883	do. [1]	−.245	.9175	.0242
128	16	−.2633	Upper [1]	.021	.7926	.4950
128	16	−.2798	Lower	−.012	.6436	.2336
128	16	−.2945	do	−.042	.6395	.1003
128	16	−.3028	do	−.080	.7194	−.0500
128	16	−.3059	do	−.104	.7634	−.0860
128	16	−.3091	do. [1]	−.185	.8804	−.1302
512	64	−.2676	Upper [1]	.018	.7536	.5779
512	64	−.2719	do	.005	.6496	.4878
512	64	−.2857	Lower	−.020	.4935	.1605
512	64	−.2926	do	−.034	.5504	.0403
512	64	−.3015	do	−.079	.6954	−.0689
512	64	−.3035	do. [1]	−.145	.8264	−.1540
2048	256	−.2737	Upper [1]	.014	.6606	.6718
2048	256	−.2748	do	.007	.5986	.5868
2048	256	−.2781		0	.5216	.4106
2048	256	−.2861	Lower	−.012	.4085	.2245
2048	256	−.2906	do	−.022	.3905	.0604
2048	256	−.2965	do	−.048	.5485	−.0967
2048	256	−.2989	do. [1]	−.100	.7584	−.1768
8192	1024	−.2798	Upper [1]	.010	.5976	.7847
8192	1024	−.2801	do	.005	------	------
8192	1024	−.2850	Lower	−.004	------	------
8192	1024	−.2886	do	−.010	.3035	.2454
8192	1024	−.2932	do	−.022	.2124	.0038
8192	1024	−.2945	do	−.030	.3423	−.0568
8192	1024	−.2958	do	−.033	.3063	−.1008
8192	1024	−.2971	do. [1]	−.065	.6765	−.1867
1024	16	−.2933	Upper [1]	.008	.4372	.8238
1024	16	−.3037	Lower [1]	−.040	.4891	−.1097
4096	64	−.2947	Upper [1]	.008	.5712	.8627
4096	64	−.3026	Lower [1]	−.024	.2221	−.1126
16384	256	−.2952	Upper [1]	.008	.5730	.9007
16384	256	−.3028	Lower [1]	−.019	.1099	−.0525

[1] Denotes tangential trajectories.

TABLE VI.—VALUES OF $C_dR/24$ AS A FUNCTION OF R

R	$C_dR/24$	R	$C_dR/24$
0	1.000	200	6.52
.05	1.009	250	7.38
.1	1.018	300	8.26
.2	1.037	350	9.00
.4	1.073	400	9.82
.6	1.108	500	11.46
.8	1.142	600	12.97
1.0	1.176	800	15.81
1.2	1.201	1,000	18.62
1.4	1.225	1,200	21.3
1.6	1.248	1,400	24.0
1.8	1.267	1,600	26.9
2.0	1.285	1,800	29.8
2.5	1.332	2,000	32.7
3.0	1.374	2,500	40.4
3.5	1.412	3,000	47.8
4.0	1.447	3,500	55.6
5.0	1.513	4,000	63.7
6.0	1.572	5,000	80.0
8.0	1.678	6,000	96.8
10.0	1.782	8,000	130.6
12	1.901	10,000	166.3
14	2.008	12,000	204
16	2.109	14,000	243
18	2.198	16,000	285
20	2.291	18,000	325
25	2.489	20,000	365
30	2.673	25,000	470
35	2.851	30,000	574
40	3.013	35,000	674
50	3.327	40,000	778
60	3.60	50,000	980
80	4.11	60,000	1175
100	4.59	80,000	1552
120	5.01	100,000	1905
140	5.40	1.2×10^5	2234
160	5.76	1.4×10^5	2549
180	6.16	1.6×10^5	2851